Cosmic ray propagation and dark matter in light of the latest AMS-02 data

JCAP09(2015)049

(http://iopscience.iop.org/1475-7516/2015/09/049)

Journal of Cosmology and Astroparticle Physics
An IOP and SISSA journal

Cosmic ray propagation and dark matter in light of the latest AMS-02 data

Hong-Bo Jin,[a,b] **Yue-Liang Wu**[a,c,d] **and Yu-Feng Zhou**[a,c]

[a]State Key Laboratory of Theoretical Physics, Institute of Theoretical Physics, Chinese Academy of Sciences, Zhong Guan Cun East Street 55 #, P.O. Box 2735, Beijing, 100190 P.R. China
[b]National Astronomical Observatories, Chinese Academy of Sciences, Datun Rd, Chaoyang, Beijing, P.R. China
[c]Kavli Institute for Theoretical Physics China, Institute of Theoretical Physics, Chinese Academy of Sciences, Zhong Guan Cun East Street 55 #, P.O. Box 2735, Beijing, 100190 P.R. China
[d]University of Chinese Academy of Sciences, Beijing, 100190 P.R. China

E-mail: hbjin@bao.ac.cn, ylwu@itp.ac.cn, yfzhou@itp.ac.cn

Received October 23, 2014
Revised July 19, 2015
Accepted August 13, 2015
Published September 21, 2015

JCAP09(2015)049

doi:10.1088/1475-7516/2015/09/049

Abstract. The AMS-02 experiment is measuring the high energy cosmic rays with unprecedented accuracy. We explore the possibility of determining the cosmic-ray propagation models using the AMS-02 data *alone*. A global Bayesian analysis of the constraints on the cosmic-ray propagation models from the preliminary AMS-02 data on the Boron to Carbon nuclei flux ratio and proton flux is performed, with the assumption that the primary nucleon source is a broken power law in rigidity. The ratio of the diffusion coefficient D_0 to the diffusive halo height Z_h is determined with high accuracy $D_0/Z_h \simeq 2.00 \pm 0.07\,\mathrm{cm^2 s^{-1} kpc^{-1}}$, and the value of the halo width is found to be $Z_h \simeq 3.3$ kpc with uncertainty less than 50%. As a consequence, the typical uncertainties in the positron fraction predicted from dark matter (DM) annihilation is reduced to a factor of two, and that in the antiproton flux is about an order of magnitude. Both of them are significantly smaller than that from the analyses prior to AMS-02. Taking into account the uncertainties and correlations in the propagation parameters, we derive conservative upper limits on the cross sections for DM annihilating into various standard model final states from the current PAMELA antiproton data. We also investigate the reconstruction capability of the future high precision AMS-02 antiproton data on the DM properties. The results show that for DM particles lighter than $\sim 100\,\mathrm{GeV}$ and with typical thermal annihilation cross section, the cross section can be well reconstructed with uncertainties about a factor of two for the AMS-02 three-year data taking.

Keywords: dark matter theory, dark matter experiments

ArXiv ePrint: 1410.0171

JCAP09(2015)049

Contents

1 Introduction

Although compelling evidence from astronomical observations has indicated that dark matter (DM) contributes to 26.8% of the total energy density of the Universe [1], the particle nature of DM remains largely unknown. If DM particles in the galactic halo can annihilate or decay into the standard model (SM) final states, they may contribute to primary sources of cosmic-ray particles, which can be probed by precision DM indirect detection experiments.

Recently, the Alpha Magnetic Spectrometer (AMS-02) collaboration has updated its measurement of the cosmic-ray positron fraction, i.e., the ratio between cosmic-ray positron flux and the total flux of electrons and positrons in the energy range of 0.5–500 GeV [2]. The high precision data indicate that the positron fraction increases with energy in the energy range 8–270 GeV, consistent with the previouse measurements by PAMELA [3, 4] and Fermi-LAT [5] but with much higher accuracy. For the first time, it was shown that the positron fraction ceases to increase at the energy ~ 270 GeV. The rise and the existence of a maximum in the positron fraction is unexpected from the conventional astrophysics in which the majority of positrons are believed to be from the collisions of primary cosmic-ray nuclei with interstellar gas. Besides astrophysical explanations, an exciting possibility is that the observed positron fraction excess is due to DM annihilation or decay in the galactic halo.

In DM interpretations, through analysing the cosmic-ray positron anomaly, the properties of DM particle such as its mass and annihilation cross section or decay life-time can be inferred, and different DM models can be distinguished or even excluded (for recent global analyses on AMS-02 data, see e.g. refs. [6–20]). However, the conclusions are in general sensitive to the choice of cosmic-ray propagation model, cosmic-ray background as well as the profile of DM halo density distribution. The main source of the uncertainty is related to that in the propagation models. Analyses based on the data prior to AMS-02 have shown that the uncertainties of this type can reach $\mathcal{O}(10)$ in the prediction for positron flux [21] and $\mathcal{O}(100)$ for anti-proton flux for DM annihilation [22]. Note that the backgrounds of primary

JCAP09(2015)049

and secondary cosmic-ray particles which are of crucial importance in identifying the DM signals also depend on the propagation models.

In the diffusion models of cosmic-ray propagation, the major propagation parameters involve the diffusion halo height Z_h, the spatial diffusion coefficient D_0, the convection velocity V_c related to the galactic wind, the Alfvèn speed V_a related to the reaccelaration, and the primary source terms, etc.. The propagation models and parameters can be constrained by a set of astrophysical observables. The ratio between the fluxes of cosmic-ray secondary and primary nuclei such as that of Boron to Carbon nuclei (B/C) and the ratio of the radioactive isotopes such as that of Beryllium nuclei ^{10}Be/^{9}Be are commonly used to determine these parameters without knowing the primary sources (for recent global fits, see e.g. [23–26]). The primary source terms can be determined separately by the fluxes of primary cosmic-ray nuclei such as that of cosmic-ray protons.

Recently, the AMS-02 collaboration has reported the measurement of the B/C ratio in the kinetic energy interval from 0.5 to 670 GeV/nucleon with an unprecedented accuracy [27]. The AMS-02 experiment also released the data of proton flux as a function of rigidity from 1 GV to 1.8 TV [28], which is consistent with the previous measurement made by PAMELA in the low rigidity range from 20 to 100 GV [29]. In the high rigidity region above ~ 100 GV, the proton spectrum measured by AMS-02 is consistent with a single power law spectrum. Under the assumption that the primary source is a broken power law in rigidity, the two type of data can be used together to determine the cosmic-ray propagation parameters.

In light of the recent significant experimental progresses, it is of interest to revisit the constraints on the cosmic-ray propagation models and explore the potential of the AMS-02 experiment on the capability of DM discovery. In this work, we first determine the main propagation parameters through a global Bayesian analysis to the preliminary AMS-02 data. We follow the strategy of determining *both* the propagation parameters and the primary sources in the same framework, using the data of B/C ratio and the proton flux. We show that the combination of B/C ratio and proton flux can lift the degeneracy in Z_h and D_0, and both the parameters can be well determined by the AMS-02 data alone. We find that the ratio of the diffusion coefficient D_0 to the diffusive halo height Z_h is determined with high accuracy $D_0/Z_h \simeq 2.00 \pm 0.07\,\mathrm{cm^2 s^{-1} kpc^{-1}}$, and the best-fit value of the halo width is $Z_h \simeq 3.3$ kpc with uncertainty within 50%. From the allowed regions of parameter space, we estimate the uncertainties in the positron fraction and antiproton fluxes predicted by DM annihilation. We show that the uncertainties in the predicted positron fraction is within a factor of two and that in the antiproton flux is within an order of magnitude, which are significantly smaller than that from the previous analyses prior to AMS-02 (see e.g. [23, 24]). We construct reference propagation models corresponding to the minimal, median and maximal antiproton fluxes from DM annihilation into b-quarks. Combined with the PAMELA antiproton data, we derive conservative upper limits on the cross sections of DM annihilating into typical SM final states. We further project the sensitivity of the forthcoming AMS-02 data on the antiproton flux. The results show that for DM particle lighter than ~ 100 GeV with a typical thermal annihilation cross section, the cross section can be reconstructed with uncertainties within a factor of two for the AMS-02 three-year data taking.

This paper is organized as follows. In section 2, we outline the formulas describing the propagation of cosmic-ray particles. In section 3, we briefly overview the method of Bayesian inference used in our analysis. In section 4, we present results on constraining the propagation models from the AMS-02 data of cosmic-ray B/C ratio and proton flux. In section 5, we discuss the uncertainties in the prediction for positron fraction from DM annihilation into

JCAP09(2015)049

typical leptonic final states. In section 6, we select typical propagation models corresponding to the minimal, median and maximal antiproton fluxes from DM annihilation into $b\bar{b}$. In section 7, taking into account the uncertainties in the propagation parameters, we derive upper limits on the DM annihilation cross sections for typical annihilation channels from PAMELA antiproton data. The reconstruction capability for the future AMS-02 data on the DM mass and annihilation cross sections is discussed. The conclusions are given in section 8.

2 Propagation of cosmic-ray charged particles

It has been recognized that the propagation of cosmic rays in the Galaxy can be effectively described as a process of diffusion [30]. In this section, we briefly overview the main features of the cosmic-ray diffusion within the Galaxy. Detailed reviews of the transportation of processes can be found in ref. [31]. The Galactic halo within which the diffusion processes occur is parametrized by a cylinder with radius $R_h = 20$ kpc and half-height $Z_h = 1$–20 kpc. The diffusion equation for the cosmic-ray charged particles reads (see e.g. [32])

$$\begin{aligned}\frac{\partial \psi}{\partial t} =& \nabla(D_{xx}\nabla\psi - \boldsymbol{V}_c\psi) + \frac{\partial}{\partial p}p^2 D_{pp}\frac{\partial}{\partial p}\frac{1}{p^2}\psi - \frac{\partial}{\partial p}\left[\dot{p}\psi - \frac{p}{3}(\nabla\cdot\boldsymbol{V}_c)\psi\right] \\ & - \frac{1}{\tau_{\rm f}}\psi - \frac{1}{\tau_{\rm r}}\psi + q(\boldsymbol{r}, p),\end{aligned} \tag{2.1}$$

where $\psi(\boldsymbol{r}, p, t)$ is the number density per unit of total particle momentum, which is related to the phase space density $f(\boldsymbol{r}, \boldsymbol{p}, t)$ as $\psi(\boldsymbol{r}, p, t) = 4\pi p^2 f(\boldsymbol{r}, \boldsymbol{p}, t)$. For steady-state diffusion, it is assumed that $\partial\psi/\partial t = 0$. The number densities of cosmic-ray particles are vanishing at the boundary of the halo, i.e., $\psi(R_h, z, p) = \psi(R, \pm Z_h, p) = 0$. The spatial diffusion coefficient D_{xx} is energy dependent and can be parametrized as

$$D_{xx} = \beta D_0 \left(\frac{\rho}{\rho_0}\right)^{\delta}, \tag{2.2}$$

where $\rho = p/(Ze)$ is the rigidity of the cosmic-ray particle with electric charge Ze. The the power spectral index δ can have different values $\delta = \delta_{1(2)}$ when ρ is below (above) a reference rigidity ρ_0. The coefficient D_0 is a normalization constant, and $\beta = v/c$ is the velocity of the cosmic-ray particle with c the speed of light. The convection term in the diffusion equation is related to the drift of cosmic-ray particles from the Galactic disc due to the Galactic wind. The direction of the wind is assumed to be along the direction perpendicular to the galactic disc plane and have opposite sign above and below the disc. The diffusion in momentum space is described by the reacceleration parameter D_{pp} which is related to the velocity of disturbances in the hydrodynamical plasma, the so called Alfvèn speed $V_{\rm a}$ as follows [32]

$$D_{pp} = \frac{4V_{\rm a}^2 p^2}{3D_{xx}\delta\,(4-\delta^2)\,(4-\delta)\,w}, \tag{2.3}$$

where w characterise the level of turbulence. We take $w = 1$ as only $V_{\rm a}^2/w$ is relevant in the calculation. In eq. (2.1), the momentum loss rate is denoted by $\dot{p}$ which could be due to ionization in the interstellar medium neutral matter, Coulomb scattering off thermal electrons in ionized plasma, bremsstrahlung, synchrotron radiation, and inverse Compton scattering, etc.. The parameter $\tau_{\rm f}(\tau_{\rm r})$ is the time scale for fragmentation (radioactive decay) of the cosmic-ray nuclei as they interact with interstellar hydrogen and helium.

JCAP09(2015)049

High energy electrons/positrons loss energy due to the processes like inverse Compton scattering and synchrotron radiation. The typical propagation length is around a few kpc for electron energy around 100 GeV. In the calculation of energy loss rate, the interstellar magnetic field in cylinder coordinates (R, z) is assumed to have the form

$$B(R,z) = B_0 \exp\left(-\frac{R-r_\odot}{R_B}\right) \exp\left(-\frac{|z|}{z_B}\right), \tag{2.4}$$

where $B_0 = 5 \times 10^{-10}$ Tesla, $R_B = 10$ kpc, $z_B = 2$ kpc [33], and $r_\odot \approx 8.5$ kpc is the distance from the Sun to the galactic center. The spectrum of a primary source term for a cosmic-ray nucleus A is assumed to have a broken power low behaviour

$$\frac{dq_A(p)}{dp} \propto \left(\frac{\rho}{\rho_{As}}\right)^{\gamma_A}, \tag{2.5}$$

with $\gamma_A = \gamma_{A1}(\gamma_{A2})$ for the nucleus rigidity ρ below (above) a reference rigidity ρ_{As}. For cosmic-ray electrons, sometimes two breaks ρ_{es1}, ρ_{es2} are introduced with three power law indices γ_{e1}, γ_{e2} and γ_{e3}. The radial distribution of the source term can be determined by independent observables. Based on the distribution of SNR, the spatial distribution of the primary sources is assumed to have the following form [34]

$$q_A(R,z) = q_0 \left(\frac{R}{r_\odot}\right)^\eta \exp\left[-\xi\frac{R-r_\odot}{r_\odot} - \frac{|z|}{0.2\,\mathrm{kpc}}\right], \tag{2.6}$$

where $\eta = 1.25$ and $\xi = 3.56$ are adapted to reproduce the Fermi-LAT gamma-ray data of the 2nd Galactic quadrant [24, 35, 36], and q_0 is a normalization parameter. In the 2D diffusion model, one can use the realistic non-uniform interstellar gas distribution of $H_{I,II}$ and H_2 determined from 21 cm and CO surveys.

Secondary cosmic-ray particles are created in collisions of primary cosmic-ray particles with interstellar gas. The secondary antiprotons are created dominantly from inelastic pp- and pHe-collisions. The corresponding source term reads

$$q(p) = \beta c n_i \sum_{i=\mathrm{H,He}} \int dp' \frac{\sigma_i(p,p')}{dp'} n_p(p') \tag{2.7}$$

where n_i is the number density of interstellar hydrogen (helium), n_p is the number density of primary cosmic-ray proton per total momentum, and $d\sigma_i(p,p')/dp'$ is the differential cross section for $p + \mathrm{H(He)} \to \bar{p} + X$.

The primary source term of cosmic-ray particles from the annihilation of Majorana DM particles has the following form

$$q(\boldsymbol{r}, p) = \frac{\rho(\boldsymbol{r})^2}{2m_\chi^2} \langle\sigma v\rangle \sum_X \eta_X \frac{dN^{(X)}}{dp}, \tag{2.8}$$

where $\langle\sigma v\rangle$ is the velocity-averaged DM annihilation cross section multiplied by DM relative velocity (referred to as cross section) which is the quantity appears in the Boltzmann equation for calculating the evolution of DM number density. $\rho(\boldsymbol{r})$ is the DM energy density distribution function, and $dN^{(X)}/dp$ is the injection energy spectrum of antiprotons from DM annihilating into SM final states through all possible intermediate states X with η_X the

JCAP09(2015)049

	α	β	γ	r_s(kpc)
NFW	1.0	3.0	1.0	20
Isothermal	2.0	2.0	0	3.5
Moore	1.5	3.0	1.5	28.0

Table 1. Values of parameters α, β, γ and r_s for three DM halo models, NFW [40], Isothermal [41], and Moore [42, 43].

corresponding branching fractions. The injection spectra $dN^{(X)}/dp$ from DM annihilation are calculated using the numerical package PYTHIA v8.175 [37], in which the long-lived particles such as neutron and K_L are allowed to decay and the final state interaction are taken into account. Since PYTHIA v8.15 the polarization and correlation of final states in τ-decays has been taken into account [38].

The fluxes of cosmic-ray particles from DM annihilation depend also on the choice of DM halo profile. N-body simulations suggest a universal form of the DM profile

$$\rho(r) = \rho_\odot \left(\frac{r}{r_\odot}\right)^{-\gamma} \left(\frac{1+(r_\odot/r_s)^\alpha}{1+(r/r_\odot)^\alpha}\right)^{(\beta-\gamma)/\alpha}, \tag{2.9}$$

where $\rho_\odot \approx 0.43$ GeV cm^{-3} is the local DM energy density [39]. The values of the parameters α, β, γ and r_s for the Navarfro-Frenk-White (NFW) profile [40], the isothermal profile [41] and the Moore profile [42, 43] are summarized in table 1. An other widely adopted DM profile is the Einasto profile [44]

$$\rho(r) = \rho_\odot \exp\left[-\left(\frac{2}{\alpha_E}\right)\left(\frac{r^{\alpha_E} - r_\odot^{\alpha_E}}{r_s^{\alpha_E}}\right)\right], \tag{2.10}$$

with $\alpha_E \approx 0.17$ and $r_s \approx 20$ kpc.

The interstellar flux of the cosmic-ray particle is related to its density function as

$$\Phi = \frac{v}{4\pi}\psi(\boldsymbol{r}, p)\ . \tag{2.11}$$

For high energy nuclei $v \approx c$. At the top of the atmosphere (TOA) of the Earth, the fluxes of cosmic-rays are affected by solar winds and the helioshperic magnetic field. This effect is taken into account using the force-field approximation [45]. In this approach, $\Phi^{\rm TOA}$ the cosmic-ray nuclei flux at the top of the atmosphere of the Earth which is measured by the experiments is related to the interstellar flux as follows

$$\Phi^{\rm TOA}(E_{\rm TOA}) = \left(\frac{2mE_{\rm TOA} + E_{\rm TOA}^2}{2mE_{\rm kin} + E_{\rm kin}^2}\right)\Phi(E_{\rm kin}), \tag{2.12}$$

where $E_{\rm TOA} = E_{\rm kin} - \phi_F$ is the kinetic energy of the cosmic-ray nuclei at the top of the atmosphere of the Earth.

Analytical solutions to the propagation equation can be obtained in a simplified two-zone diffusion model in which the thin galactic disk is approximated by a delta-function $\delta(z)$ (for reviews, see e.g. [31]). For an illustration, let us consider a simple case where the reacceleration and energy loss terms are negligible, and V_c is a constant along the z-direction. The steady state propagation equation in this case can be written as

$$0 = D_{xx}\nabla^2\psi - V_c\nabla\psi - 2h\delta(z)\frac{1}{\tau_{\rm f}}\psi - \frac{1}{\tau_{\rm r}}\psi + 2h\delta(z)q(R,z,p). \tag{2.13}$$

JCAP09(2015)049

where $h \approx 0.1$ kpc is the half-height of the galactic disk used as a normalization factor. Using the Bessel expansion of the number density

$$\psi(R, z, p) = \sum_{i=1}^{\infty} \psi_i(z, p) J_0\left(\zeta_i \frac{R}{R_h}\right), \tag{2.14}$$

where $J_0(x)$ is the zero-th order Bessel function of the first kind and ζ_i is the i-th zero of the Bessel function, the equation for the coefficients $\psi_i(z, p)$ can be written as

$$0 = D_{xx}\left(\frac{\partial^2}{\partial z^2} - \frac{\zeta_i^2}{R_h^2}\right)\psi_i - V_c \frac{\partial}{\partial z}\psi_i - 2h\delta(z)\frac{1}{\tau_{\rm f}}\psi_i - \frac{1}{\tau_{\rm r}}\psi_i + 2h\delta(z)q_i, \tag{2.15}$$

where q_i are the coefficients of the Bessel expansion of the source term $q(R, z, p)$ similar to ψ_i in eq. (2.14). The solution of the above equation at $z = 0$ is given by [31]

$$\psi_i(0) = \frac{2hq_i}{V_c + 2h/\tau_{\rm f} + D_{xx} S_i \coth(S_i Z_h/2)}, \tag{2.16}$$

where

$$S_i^2 = \frac{V_c^2}{D_{xx}^2} + \frac{4}{D_{xx}\tau_{\rm r}} + \frac{4\zeta_i^2}{R_h^2}. \tag{2.17}$$

In the limit $S_i Z_h \ll 1$ which is valid at sufficiently high energy, one can use the power expansion $\coth(x) \approx 1/x + x/3 + \mathcal{O}(x^3)$ and obtain

$$D_{xx} S_i \coth(S_i Z_h/2) \approx \left(\frac{D_{xx}}{Z_h}\right)\left(2 + \frac{V_c^2 Z_h^2}{6D_{xx}^2} + \frac{2Z_h^2}{3D_{xx}\tau_{\rm r}} + \frac{2Z_h^2}{3R_h^2}\zeta_i^2\right). \tag{2.18}$$

Since $D_{xx} \propto D_0$, the above expression shows the well-known behaviour that the parameters D_0 and Z_h are almost degenerate. This degeneracy is however slightly lifted by the two subleading contributions. One is related to the decay of the radioactive species, and the other one is related to the fixed halo radius R_h which is common to all the cosmic-ray species. The values of D_0 and Z_h can be determined by fitting simultaneously to the B/C flux ratio and the ratio of the isotopes of Beryllium nuclei ^{10}Be/^{9}Be, as ^{10}Be is radioactive and its propagation is directly sensitive to D_0. An advantage of using such flux ratios is that the propagation parameters can be determined without the knowledge of the primary sources. On the other hand, as shown in eq. (2.18), for a fixed value of D_0/Z_h, an increase of Z_h will result in a slight decrease of the flux ψ_i even for stable cosmic-ray species. Therefore, the stable primary cosmic-ray fluxes such as the proton flux can also be used together with the B/C flux ratio to determine the values of Z_h, provided that the primary sources are specified and the data are precision enough.

The energy spectrum of the proton flux is known to follow a single power law $\psi(0) \propto \rho^{-\gamma_\psi}$ in the energy range $\mathcal{O}(20\text{–}10^7)$ GeV with $\gamma_\psi \approx 2.7$. Since $D_{xx} \propto \rho^\delta$, according to the solution of eq. (2.16), if the rigidity dependence of the source term is also a single power law $q_i \propto \rho^{-\gamma}$, then at high energies the approximate relation $\gamma_\psi \approx \gamma + \delta$ follows, which means that for the proton spectrum the two parameters γ and δ are nearly degenerate. However, at lower energies $E_{\rm kin} \lesssim 20$ GeV, the single power-law approximation of the proton energy spectrum breaks down. The energy redistribution processes such as reacceleration, convection and solar modulation, etc. contribute to the changes in the spectral shape of the proton flux. Thus

JCAP09(2015)049

γ and δ can be determined individually by the proton flux together with other propagation parameters. Furthermore, the primary proton source term can also be a broken power law in rigidity as widely adopted in the diffusive re-acceleration models [24, 46, 47], which is also suggested independently by the γ-ray observation of the nearby molecular clouds [48]. As it will be shown in detail in section 4, the combination of proton flux plus B/C ratio can break the degeneracies between the parameters, and allows for a determination of the propagation parameters D_0, Z_h, $V_{\rm a}$, $\gamma_{p1,p2}$ and δ etc. with reasonable precisions.

In our numerical calculations, we shall solve the diffusion equation of eq. (2.1) using the publicly available code GALPROP v54 [35, 46, 47, 49, 50] which utilizes realistic astronomical information on the distribution of interstellar gas and other data as input, and considers various kinds of data including primary and secondary nuclei, electrons and positrons, γ-rays, synchrotron radiation, etc. in a self-consistent way. Other approaches based on simplified assumptions on the Galactic gas distribution which allow for fast analytic solutions can be found in refs. [22, 23, 31, 51, 52]. The propagation parameters shall be determined from a global fit using Bayesian inference with Markov Chain Monte-Carlo method.

3 Bayesian inference

The Bayesian inference is based on calculating the posterior probability distribution function (PDF) of the unknown parameter set $\boldsymbol{\theta} = \{\theta_1, \ldots, \theta_m\}$ in a given model, which actually updates our state of belief from the prior PDF of $\boldsymbol{\theta}$ after taking into account the information provided by the experimental data set D. The posterior PDF is related to the prior PDF by the Bayes's therom

$$p(\boldsymbol{\theta}|D) = \frac{\mathcal{L}(D|\boldsymbol{\theta})\pi(\boldsymbol{\theta})}{p(D)}, \tag{3.1}$$

where $\mathcal{L}(D|\boldsymbol{\theta})$ is the likelihood function, and $\pi(\boldsymbol{\theta})$ is the prior PDF which encompasses our state of knowledge on the values of the parameters before the observation of the data. The quantity $p(D)$ is the Bayesian evidence which is obtained by integrating the product of the likelihood and the prior over the whole volume of the parameter space

$$p(D) = \int_V \mathcal{L}(D|\theta)\pi(\boldsymbol{\theta})d\theta. \tag{3.2}$$

The evidence is an important quantity for Bayesian model comparison. It is straight forward to obtain the marginal PDFs of interested parameters $\{\theta_1, \ldots, \theta_n\}(n < m)$ by integrating out other nuisance parameters $\{\theta_{n+1}, \ldots, \theta_m\}$

$$p(\theta_1, \ldots, \theta_n)_{\rm marg} = \int p(\boldsymbol{\theta}|D) \prod_{i=n+1}^{m} d\theta_i. \tag{3.3}$$

The marginal PDF is often used in visual presentation. If there is no preferred value of θ_i in the allowed range $(\theta_{i,\rm min}, \theta_{i,\rm max})$, the priors can be taken as a flat distribution

$$\pi(\theta_i) \propto \begin{cases} 1, & \text{for } \theta_{i,\rm min} < \theta_i < \theta_{i,\rm max} \\ 0, & \text{otherwise} \end{cases}. \tag{3.4}$$

JCAP09(2015)049

The likelihood function is often assumed to be Gaussian

$$\mathcal{L}(D|\boldsymbol{\theta}) = \prod_i \frac{1}{\sqrt{2\pi\sigma_i^2}} \exp\left[-\frac{(f_{\mathrm{th},i}(\boldsymbol{\theta}) - f_{\mathrm{exp},i})^2}{2\sigma_i^2}\right], \tag{3.5}$$

where $f_{\mathrm{th},i}(\boldsymbol{\theta})$ are the predicted i-th observable from the model which depends on the parameter set $\boldsymbol{\theta}$, and $f_{\mathrm{exp},i}$ are the ones measured by the experiment with uncertainty σ_i. For experiments with only a few events observed, the form of the likelihood function can be taken as Poisson. When the form of the likelihood function is specified, the posterior PDF can be determined by sampling the distribution according to the prior PDF and the likelihood function using Markov Chain Monte Carlo (MCMC) methods. A commonly adopted algorithm is Metropolis-Hastings MCMC which is implemented in the numerical package `CosmoMC` [53]. Other advanced sampling methods such as the `MultiNest` algorithm are also commonly adopted [54, 55].

The statistic mean value of a parameter θ can be obtained from the posterior PDF $P(\boldsymbol{\theta}|D)$ in a straight forward manner. Using the MCMC sequence $\{\theta_i^{(1)}, \theta_i^{(2)}, \ldots, \theta_i^{(N)}\}$ of the parameter θ_i with N the length of the Markov chain, the mean (expectation) value $\langle\theta_i\rangle$ is given by

$$\langle\theta_i\rangle = \int \theta_i P(\theta_i|D) d\theta_i = \frac{1}{N}\sum_{k=1}^{N} \theta_i^{(k)}. \tag{3.6}$$

The 1σ standard deviation of the parameter θ_i is given by $\sigma^2 = \sum_{k=1}^{N}(\theta_i^{(k)} - \langle\theta_i\rangle)^2/(N-1)$.

4 Constraining propagation models using AMS-02 data

The propagation models can be constrained by cosmic-ray data. Since the statistics of the AMS-02 data on charged cosmic-ray particles are now much higher than that of other experiments and will continue to increase, it is of interest to consider constraining the propagation models using the AMS-02 data alone. One advantage of this strategy is that the complicities involving the combination of the systematics of different type of experiments can be avoided. Furthermore, all the current AMS-02 data are taken in the same period of solar activity, which makes it easier to estimate the effect of solar modulation consistently.

The AMS-02 data of which we shall include in the analysis are the spectra of the cosmic-ray nuclei ratio B/C (18 data points) [27] and the proton flux (100 data points) [28], namely, the whole data set is

$$D = \{D_{B/C}^{\mathrm{AMS}}, D_p^{\mathrm{AMS}}\}. \tag{4.1}$$

Note that the current data released by the AMS-02 collaboration is still preliminary, which can be different from the final published results.

Since we are focusing on determining the propagation parameters, the AMS-02 data of positrons and electrons [56] are not considered for the moment, as it is known that they are unlikely to be fully consistent with the conventional backgrounds, which calls for exotic contributions either from nearby astrophysical sources or from DM interactions.

We adopt the conventional diffusive reaccelaration (DR) models in which $V_c \simeq 0$. It has been shown that in the GALPROP approach a nonvanishing V_c results in the predicted peak

JCAP09(2015)049

of B/C spectrum to be too wide in comparison with the data [35, 46]. We consider the case where $R = 20$ kpc and $\delta_1 = \delta_2 \equiv \delta$, thus there are 4 free parameters related to the cosmic-ray propagation: Z_h, D_0, δ and V_a. Two additional parameters γ_{p1} and γ_{p2} are introduced for the power-law indices of the primary source terms. The break in rigidity of the primary source is fixed at $\rho_{ps} = 10^4$ MV. In the GALPROP code, the primary nuclei source term is normalized in such a way that the proton flux N_p at a reference kinetic energy $E_{\rm kin}$ =100 GeV is reproduced. We find $N_p = 4.83 \pm 0.02\,{\rm cm^{-2}sr^{-1}s^{-1}MeV^{-1}}$ from interpolating the AMS-02 proton flux data at 100 GeV. The solar modulation amplitude ϕ which affects the low energy spectra of the cosmic ray particles correlates strongly with the power-law index γ_{p1}. Fitting both ϕ and γ_{p1} simultaneously will significantly slow down the convergence of the MCMC sampling. Thus, in this work we fix the value of ϕ at $\phi = 550$ MV. As a cross check, after the global fit, we performed a number of fits with other choices of ϕ. The result shows that the lowest χ^2 corresponds to $\phi \approx 542$ MV, which is close to the value we adopted. Thus in total there are 6 free parameters

$$\boldsymbol{\theta} = \{Z_h, D_0, \delta, V_a, \gamma_{p1}, \gamma_{p2}\}. \tag{4.2}$$

The priors of all the parameters are chosen to be uniform distributions according to eq. (3.4) with the prior intervals shown in table 2.

In the GALPROP code, the diffusion equation is solved numerically on a spatial grid with widths $\Delta R = 1$ kpc and $\Delta Z = 0.2$ kpc. The momentum grid is on a logarithmic scale with a scale factor 1.4. For sampling the posterior distributions and calculating the marginal distributions, we use the numerical package `CosmoMC` [53] which implements the Metropolis-Hastings algorithm in the MCMC scan of the whole parameter space. We have built 18 parallel MCMC chains with ∼1500 samples in each chain after burn-in. These chains satisfy the convergence condition that the ratio of the inter-chain variance and intra-chain variance is less than 0.2 [57]. In total 2.6×10^4 samples were obtained from the MCMC scan. The results of the best-fit values, statistical mean values, standard deviations and allowed intervals at 95% confidence level (CL) for these parameters are summaried in table 2. For a comparison, we also list the allowed ranges determined from a previous analysis in ref. [24] which is based on the data prior to AMS-02 such as the B/C ratio from HEAO-3 [58], ATIC-2 [59] and CREAM-1 [60], the data of ^{10}B/^{9}Be from ACE [61], and the data of Carbon and Oxygen nuclei fluxes from ACE [62]. For an estimate of the goodness-of-fit, we evaluate the χ^2 function which is defined as $\chi^2 = -2\ln\mathcal{L}$. Using the best-fit parameters, we find that in total $\chi^2 = 49.0$ in which the contribution from B/C is 6.1 and that from proton flux is 42.9. Thus $\chi^2/{\rm dof} = 49.0/112$ which indicates a good agreement with the data.

As it can be seen from the table, although the fitting strategy is quite different, the parameters determined by the AMS-02 data are similar to that in ref. [24], but the uncertainties in the parameters are significantly smaller. For instance, the ratio D_0/Z_h is found to be

$$\frac{D_0}{Z_h} = (2.00 \pm 0.07)\,{\rm cm^2 s^{-1} kpc^{-1}}. \tag{4.3}$$

The uncertainty is within 5%, which is mostly constrained by the B/C data. Note that a relatively small halo height is favoured by the AMS-02 data

$$Z_h = 3.3 \pm 0.6\,{\rm kpc}. \tag{4.4}$$

JCAP09(2015)049

Quantity	Prior range	Best-fit value	Posterior mean and Standard deviation	Posterior 95% range	Ref. [24]
Z_h(kpc)	[1, 11]	3.2	3.3±0.6	[2.1, 4.6]	5.4±1.4
D_0/Z_h	[1, 3]	2.02	2.00±0.07	[1.82, 2.18]	(1.54±0.48)
δ	[0.1, 0.6]	0.29	0.29±0.01	[0.27, 0.32]	0.31±0.02
$V_a(\mathrm{km\cdot s^{-1}})$	[20, 70]	44.7	44.6±1.2	[41.3, 47.5]	38.4±2.1
γ_{p1}	[1.5, 2.1]	1.79	1.78±0.01	[1.75, 1.81]	1.92±0.04
γ_{p2}	[2.2,2.6]	2.46	2.45±0.01	[2.43,2.47]	2.38±0.04

Table 2. Constraints on the propagation models from the global Bayesian analyses to the AMS-02 data of B/C ratio and proton flux. The prior interval, best-fit value, statistic mean, standard deviation and the allowed range at 95% CL are listed for each propagation parameter. The parameter D_0/Z_h is in units of $10^{28}\mathrm{cm^2\cdot s^{-1}kpc^{-1}}$. For a comparison, we also list the mean values and standard deviations of these parameters from a previous analysis in [24]. The value of D_0/Z_h in the parentheses is obtained from [24] using a naive combination of D_0 and Z_h without considering the correlation.

Compared with $Z_h = 5.4 \pm 1.4\,\mathrm{kpc}$ obtained in ref. [24], the value of Z_h from this work is $\sim 40\%$ lower with the uncertainty smaller by a factor of two. A previous MCMC fit based on the two-zone diffusion model gives $Z_h = 8^{+8}_{-7}$ kpc [23].

While the ratio D_0/Z_h is sensitive to the B/C ratio, the absolute value of Z_h is more sensitive to the proton flux. For an illustration of the Z_h dependence, it is useful to define a relative deviation of an observable $\psi(D_0, Z_h)$ from a reference value $\psi(\hat{D}_0, \hat{Z}_h)$ as follows

$$\epsilon_1(D_0, Z_h) \equiv \frac{\psi(D_0, Z_h) - \psi(\hat{D}_0, \hat{Z}_h)}{\psi(\hat{D}_0, \hat{Z}_h)}, \tag{4.5}$$

where ψ can be the proton flux or the B/C flux ratio. We choose $\hat{D}_0$ and $\hat{Z}_h$ to be the best-fit value of the diffusion coefficient and the halo half-height listed in table 2. Using the GALPROP code, we show in figure 1 how the value of $\epsilon_1(D_0, Z_h)$ changes with Z_h for the proton flux and B/C flux ratio, under the constraint that $D_0/Z_h = \hat{D}_0/\hat{Z}_0$, at a reference kinetic energy $E_{\mathrm{kin}} = 24.2\,\mathrm{GeV/n}$ with all the other parameters fixed at their best-fit values listed in table 2. The option `proton_norm_flux=0` is used to prevent the GALPROP code from automatically normalizing the proton flux to N_p. If there exists an exact D_0/Z_h degeneration, it is expected that $\epsilon_1(D_0, Z_h)$ is vanishing for all the value of Z_h. However, as shown in the upper panels of figure 1, the proton flux decreases by $\sim 9\%$ in the Z_h interval 2.2–4.2 kpc for $R_h = 20$ kpc. The decrease of the proton flux with an increasing Z_h is consistent with eq. (2.18). The uncertainties in the data of the proton flux are dominated by the systematic uncertainties in the acceptance ($\sim 2.8\%$), trigger efficiency ($\sim 1.0\%$) and proton track efficiency ($\sim 1.0\%$) [28]. The total systematic uncertainty added up together is $\sim 3.1\%$, which is also shown in figure 1 for a comparison. One can see that such a precision measurement on the proton flux can place an useful constraint on Z_h. On the other hand, the Z_h dependence of the B/C ratio is relatively small. The β-decay of $^{10}\mathrm{Be} \to {}^{10}\mathrm{B}$ may introduce another Z_h dependence in the B/C ratio, as discussed in ref. [23]. The uncertainty in the data of the B/C ratio is $\sim 4\%$ at $E_{\mathrm{kin}} \sim 20$ GeV/n [27], which is less stringent in constraining the value of Z_h.

In this work, we fix the value of $R = 20$ kpc in order to facilitate the comparisons with other analyses, especially that in refs. [23, 24]. It is anyway useful to examine whether the

JCAP09(2015)049

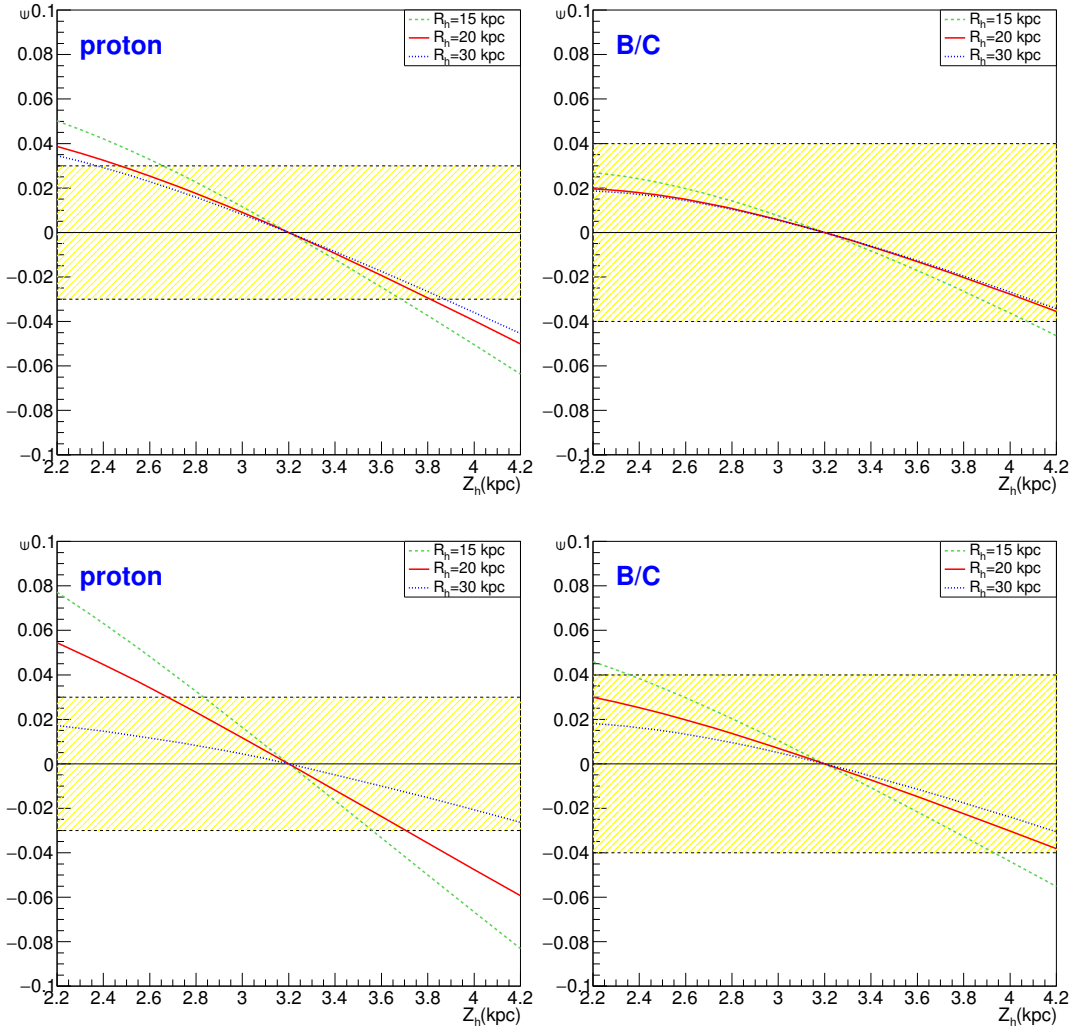

Figure 1. Upper panels) Relative deviation ϵ_1 of proton flux (upper left) and B/C ratio (upper right) as a function of the halo half-height Z_h at the kinetic energy $E_{\rm kin} = 24.2\,{\rm GeV/n}$, for three choices of $R_h = 15$, 20 and 30 kpc, respectively. The ratio D_0/Z_h and other parameters are fixed at their best-fit values given in table 2. The spatial distribution of the primary source is taken from eq. (2.6). The calculation is done using the GALPROP code. The horizontal bands represent the uncertainties of the AMS-02 data at around 20 GeV [28]. Lower panels) The same as in the upper panels, but with an uniform distribution of the primary source term.

Z_h dependence of the related observables can be affected by different choices of R_h and the spatial distributions of the primary source term. In figure 1, we also show the results for $R_h = 15$ and 30 kpc, respectively. In all the three cases, it is found that the value of ϵ_1 is nonvanishing and depends on Z_h. For a larger $R_h = 30$ kpc, the changes in ϵ_1 for proton flux are slightly smaller, while for a smaller $R_h = 15$ kpc, the changes in ϵ_1 are larger and can reach $\sim 11\%$ in the Z_h interval 2.2–4.2 kpc. The changes in the value of ϵ_1 in the B/C flux ratio follow the similar trend. The spatial distribution of the primary source can be determined by independent observables such as the Galactic diffuse γ-rays. In the GALPROP code, the source distribution is adopted to reproduce the Fermi-LAT γ-ray data of the 2nd Galactic quadrant [36]. For a comparison, we consider a simplified case where the primary source is uniformly distributed along the R-direction. The corresponding results on the variation

JCAP09(2015)049

of ϵ_1 are shown in the lower panels of figure 1. One can see that the Z_h dependences are more significant than the case where the source term is described by eq. (2.6). These results suggest that the breakdown of the D_0/Z_h degeneracy by the proton flux may be a generic feature of the two-dimensional diffusion models.

Complementary constraints on Z_h can be obtained from the synchrotron emission of the Galaxy [63–66]. The conclusion inevitably depends on the assumption on the strength and distribution of the Galactic magnetic field B which are largely unknown. Assuming an uniform $B = 6.5\ \mu G$, it was found that 1 kpc $\lesssim Z_h \lesssim$ 15 kpc in the two-zone diffusion model [65]. A GALPROP based calculation with a spatial-dependent B field and including an anisotropic component favoured a halo size around 10 kpc [64]. An analysis using the DRAGON code with spatial-dependent D_{xx} and B favoured $Z_h \gtrsim 6$ kpc [63]. Using the low energy electron/positron flux, is was found that the PAMELA data disfavoured $Z_h \lesssim$ 3 kpc [67]. But significant uncertainties can arise from dealing with the effects of the solar modulation.

The determined power-law index in the diffusion term is $\delta = 0.29 \pm 0.01$ which is smaller than $\delta \approx 0.7$ from the analysis based on the two-zone diffusion model [68], but is consistent with 0.31 ± 0.02 from the previous GALPROP based global fit [24] and is very close to 1/3 from the Kolmogorov-type spectrum. Since the prior range for δ is set to be 0.1–0.6 which is much wider than the favoured range of δ at 95% CL, the determined value of δ is insensitive to the choice of prior distribution. The power-law indices of the nuclei source term are found to be $\gamma_{p1} = 1.78 \pm 0.01$ and $\gamma_{p2} = 2.45 \pm 0.01$, respectively. As emphasized in section 2, the low energy spectrum of the proton flux can be used to lift the degeneracy between γ_{p2} and δ. Similar to the quantity ϵ_1, one can define a relative change in the proton flux as a function of γ_{p2} and δ as follows

$$\epsilon_2(\gamma_{p2}, \delta) \equiv \frac{\psi(\gamma_{p2}, \delta) - \psi(\hat{\gamma}_{p2}, \hat{\delta})}{\psi(\hat{\gamma}_{p2}, \hat{\delta})}, \tag{4.6}$$

where $\hat{\gamma}_{p2}$ and $\hat{\delta}$ are the best-fit values given in table 2. We show in the left panel of figure 2 the value of $\epsilon_2(\gamma_{p2}, \delta)$ as a function of δ, under the constraint $\gamma_{p2} + \delta = \hat{\gamma}_{p2} + \hat{\delta} = 2.74$. If there exists an exact degeneracy in γ_{p2} and δ, it is expected that ϵ_2 will be vanishing. However, as can be seen from figure 2, at $E_{\rm kin} = 24.2\,{\rm GeV}$, the value of ϵ_2 is not vanishing, and the change in ϵ_2 is more than $\sim 10\%$ when δ increases from 0.265 to 0.315. At higher energies $E_{\rm kin} = 103$ and 700 GeV, the changes in ϵ_2 become smaller, which is consistent with the fact that the proton energy spectrum is closer to a single power law at high energies. A stronger ϵ_2 dependence is found in the B/C flux ratio as shown in the right panel of figure 2, which indicates that the value of δ can be constrained by the B/C ratio.

Based on the MCMC samples, the contours of allowed regions at 68% and 95% CL for a selection of propagation parameters are shown in figure 3. Some of the determined parameters are strongly correlated. For instance, D_0/Z_h is negatively correlated with δ, which is expected from the analytical solution of eq. (2.16). The parameter δ is negatively correlated with γ_{p1} and γ_{p2}, which is also consistent with eq. (2.16), as the sum $\delta + \gamma_{p1}(\gamma_{p2})$ should roughly reproduce the observed proton energy spectrum at low (high) energies. The Alfvèn speed $V_{\rm a}$ is found to be positively correlated with D_0/Z_h, which can be understood from the definition of the re-acceleration term in eq. (2.3). Less pronounced correlations are found between parameters $V_{\rm a}$ and $\gamma_{p1,p2}$. The one-dimensional marginal posterior PDFs for some of the parameters are shown in figure 4. In the figure, the best-fit values, mean values with standard deviations are also shown.

JCAP09(2015)049

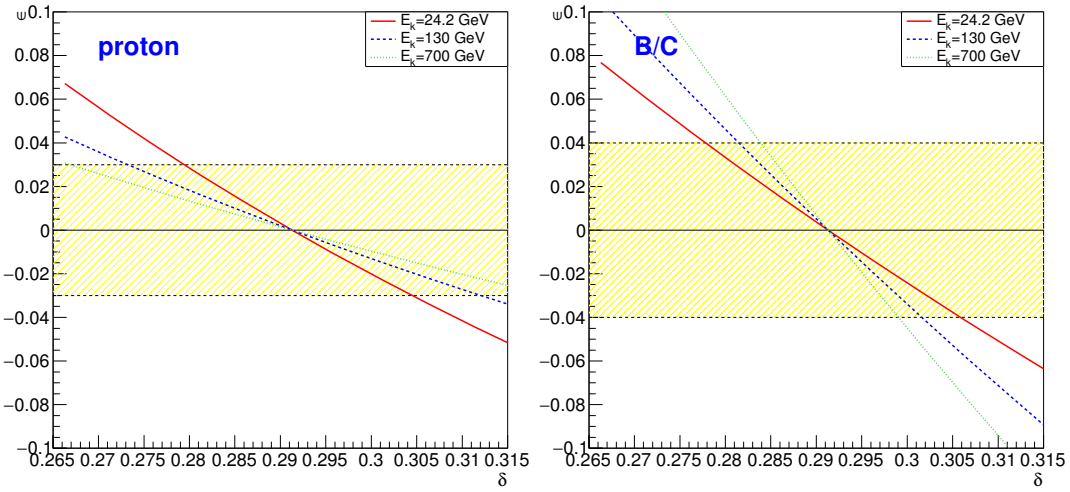

Figure 2. Left) Relative deviation ϵ_2 of proton flux as a function of the power law index δ in the diffusion coefficient, under the condition $\gamma_{p2} + \delta = 2.74$, for three values of kinetic energy $E_{\rm kin} = 24.2$, 130, and 700 GeV/n, respectively. Other parameters are fixed at their best-fit values given in table 2. The calculations are done using the GALPROP code. The horizontal band represents the uncertaintie of the AMS-02 data at around 20 GeV [28]. Right) The same as Left but for the B/C flux ratio.

Figure 5 shows the fitted spectra of the proton flux and B/C ratio, and the predicted antiproton fluxe, antiproton/proton ratio and ^{10}Be/Be ratio using the parameters allowed within 95% CL. The AMS-02 data on proton flux and B/C ratio are well reproduced by the GALPROP DR models. Although the Z_h is determined purely by the proton flux, the predicted ^{10}Be/Be ratio is consistent with the data of ACE [61] and ISOMAX [69]. The predicted antiproton fluxes are consistent with the PAMELA data only for the kinetic energies above 10 GeV. At lower energies, the predicted antiproton flux is about 40% lower than the data of PAMELA and BESS-Polar II, which is a typical feature of the DR models in GALPROP [46]. The low energy antiproton spectrum can be correctly reproduced if one constructs sophisticated GALPROP models with a flattening of the diffusion coefficient together with a convection term and a break in the injection spectrum [46]. Another possibility is that the solar modulation may have a charge sign dependence, namely, the modulation for antiprotons is different from that of protons.

5 Positron fraction from DM annihilation

Recently the measurement of the positron fraction was extended to the energy range up to 500 GeV by AMS-02 [2]. For the first time, it was shown that the positron fraction stops to increase with energy at ~ 270 GeV. The spectral features of the positron fraction such as the rate of increase with energy, the energy beyond which it ceases to increase and the rate at which it falls beyond the turning point are of crucial importance in distinguishing the DM models. Since the uncertainties in the propagation parameters affect the calculations of *both* the background and the DM contribution in the positron fraction, it is necessary to consider this uncertainty in deriving the properties of DM particles from the positron excess.

We first investigate the predicted positron fraction for the case of background only. The result is shown in figure 5, where we have chosen a reference electron primary source with two breaks at $\rho_{e1} = 4$ GV and $\rho_{e2} = 86.8$ GV, and three power law indices between

JCAP09(2015)049

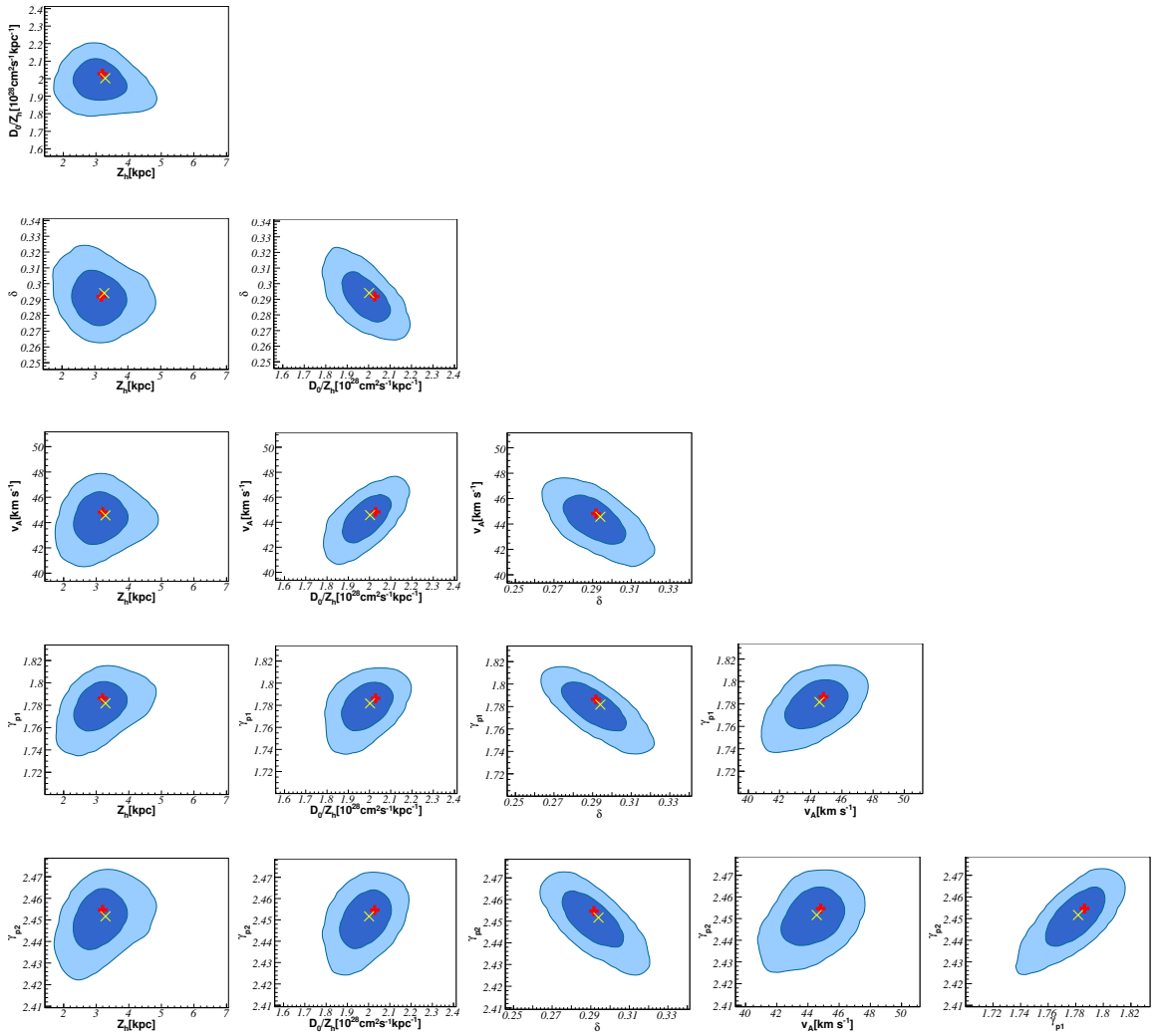

Figure 3. Two-dimensional marginalized posterior PDFs for the combinations of some selected parameters involving Z_h, D_0/Z_h, δ, V_a and γ_{p1}. The regions enclosing 68%(95%) CL are shown in dark blue (blue). The red plus (yellow cross) in each plot indicates the best-fit value (statistic mean value).

the breaks: $\gamma_{e1} = 1.46$, $\gamma_{e2} = 2.72$ and $\gamma_{e3} = 2.49$, respectively. The shaded bands in the figure correspond to the variation of the propagation parameters within 95% CL. The figure shows that the typical uncertainties in the positron fraction can reach a factor of two in the background-only case. Clearly, at energies above $\sim 20\,\mathrm{GeV}$, the positron fraction cannot be explained by the background even after including the uncertainties of the propagation parameters, which calls for exotic contributions such as halo DM annihilation.

We then include the DM contribution and add the AMS-02 data of positron fraction into a similar global Bayesian fit detailed in section 3 to determine the DM particle mass m_χ and annihilation cross section $\langle\sigma v\rangle$ for various DM annihilation channels. The major propagation parameters such as Z_h, D_0/Z_h, V_a, δ, γ_{p1} and γ_{p2} are also allowed to vary freely as nuisance parameters in the fit. In order to avoid the uncertainties related to the modelling of Solar modulation, only the positron fraction data with kinetic energy above 20 GeV are included in the fit. For the four typical DM annihilation channels $\chi\bar{\chi} \to 2\mu$, 4μ, 2τ and 4τ

JCAP09(2015)049

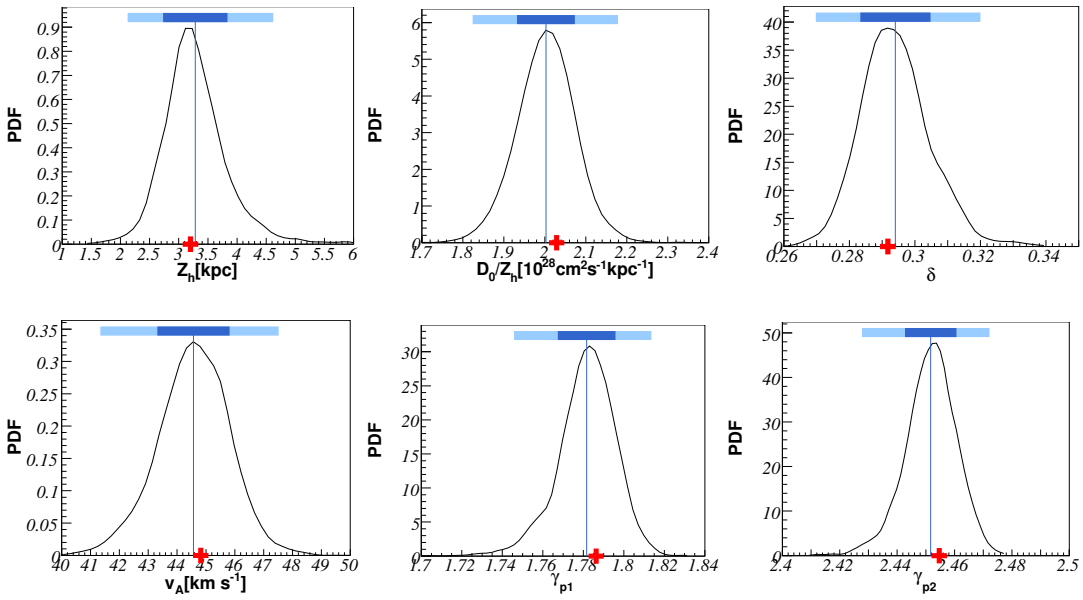

Figure 4. One-dimensional marginalized posterior PDFs for propagation parameters Z_h, D_0/Z_h, δ, V_a, γ_{p1}, γ_{p2}. In each panel, the horizontal bar indicates the 1σ- and 2σ-standard deviations, with vertical line indicating the statistic mean value. The best-fit value is shown as red plus.

with the Einasto DM profile, we find the following results

$$
\begin{aligned}
2\mu &: m_\chi = 507 \pm 30 \text{ GeV}, && \langle\sigma v\rangle = (1.72 \pm 0.14) \times 10^{-24}\,\text{cm}^3\text{s}^{-1},\\
4\mu &: m_\chi = 903 \pm 50 \text{ GeV}, && \langle\sigma v\rangle = (3.28 \pm 0.24) \times 10^{-24}\,\text{cm}^3\text{s}^{-1},\\
2\tau &: m_\chi = 1076 \pm 100 \text{ GeV}, && \langle\sigma v\rangle = (1.03 \pm 0.10) \times 10^{-23}\,\text{cm}^3\text{s}^{-1},\\
4\tau &: m_\chi = 1964 \pm 224 \text{ GeV}, && \langle\sigma v\rangle = (2.06 \pm 0.23) \times 10^{-22}\,\text{cm}^3\text{s}^{-1}.
\end{aligned}
\tag{5.1}
$$

The allowed regions in the $(m_\chi, \langle\sigma v\rangle)$ plane at 99% CL are shown in figure 6. The corresponding values of χ^2/d.o.f which indicate the goodness-of-fit are 2.92 (2μ), 2.16 (4μ), 1.44 (2τ) and 1.27 (4τ), respectively. In figure 7, we show the predicted positron fraction for the four typical DM annihilation channels with the Einasto DM profile. The band in each plot indicates the uncertainties due to both the DM parameters and the propagation parameters at 95% CL. One can see from the the figure that for the channels with μ final states the predicted spectra are too hard to fit the AMS-02 data at high energies. Thus the τ final states are favoured over μ final states by the AMS-02 data. However, the cross sections for τ final states are very large and in strong tension with the gamma-ray bound from the dwraf spheroid satellite galaxies of the Milky Way [75] as can be seen from the figure. These result are consistent with our previous work using the earlier AMS-02 data and a set of fixed backgrounds [11].

6 Antiproton flux from DM annihilation

Compared with cosmic-ray electrons, which loss energy quickly due to the inverse Compton scattering and synchrotron radiation, the cosmic-ray protons lose much less energy in the propagation process. Thus they can travel across a longer distance in the galaxy before

JCAP09(2015)049

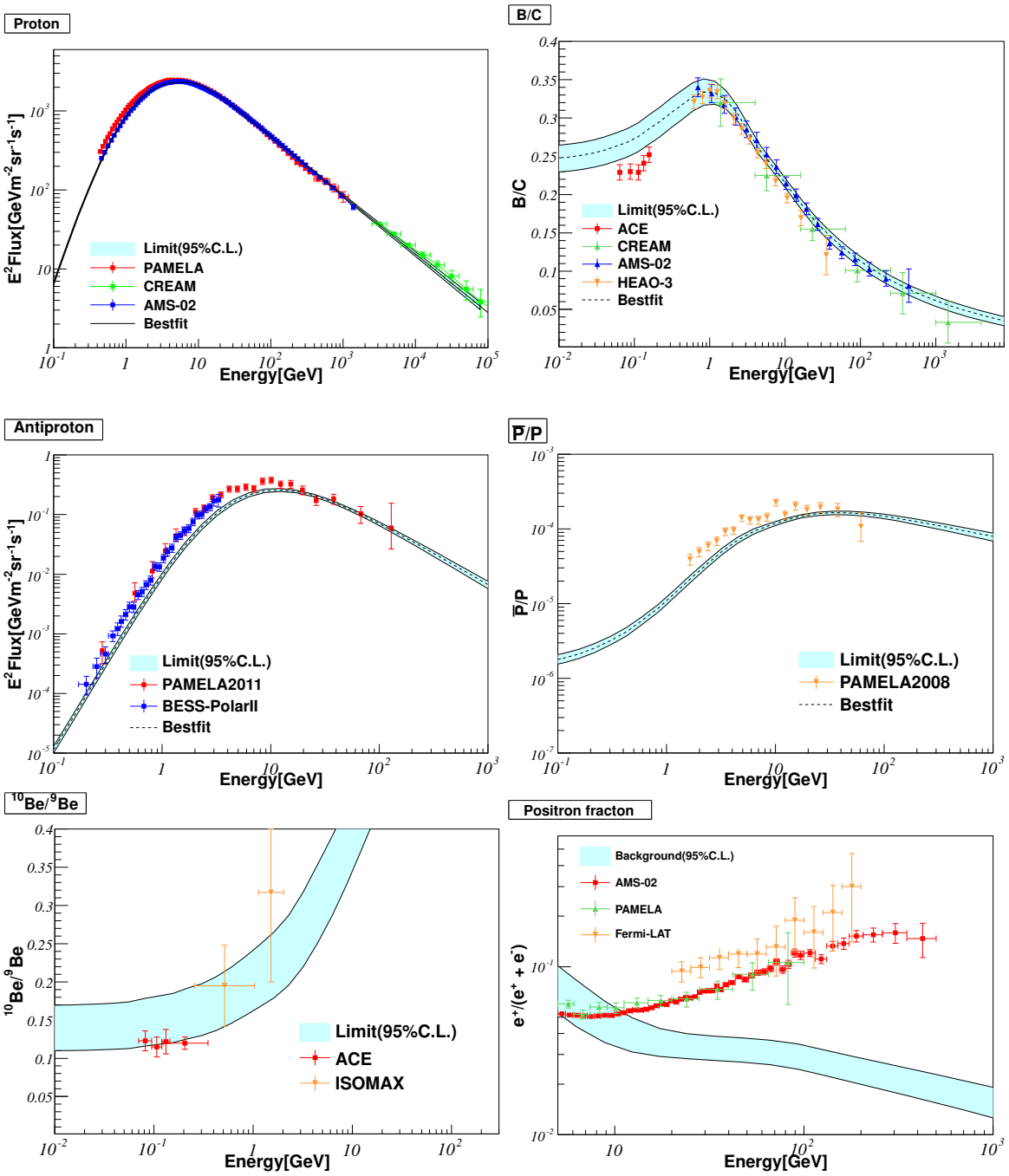

Figure 5. Cosmic ray nuclei fluxes and flux ratios from a global fit to the AMS-02 proton and B/C data. (Upper left) the fitted spectra of cosmic-ray proton flux. The band corresponds to the values of propagation parameters allowed at 95% CL. The data of proton flux from AMS-02 [28], PAMELA [29] and CREAM [70] are also shown. (Upper right) the fitted spectra of B/C ratio. The data of AMS-02 [27], ACE [71], CREAM [60] and HEAO-3 [58] are also shown. (Middle left) the prediction for the antiproton flux at 95% CL. The data of PAMELA [72] and BESS-Polar II [73] are shown. (Middle right) the prediction for the antiproton to proton flux ratio at 95% CL. The data of PAMELA [74] are shown. (Lower left) the prediction for ^{10}Be/^{9}Be flux ratio, the data of ACE [61] and ISOMAX [69] are shown. (Lower right) the prediction for positron fraction, the data of AMS-02 [2] PAMELA [4] and Fermi-LAT [5] are shown.

JCAP09(2015)049

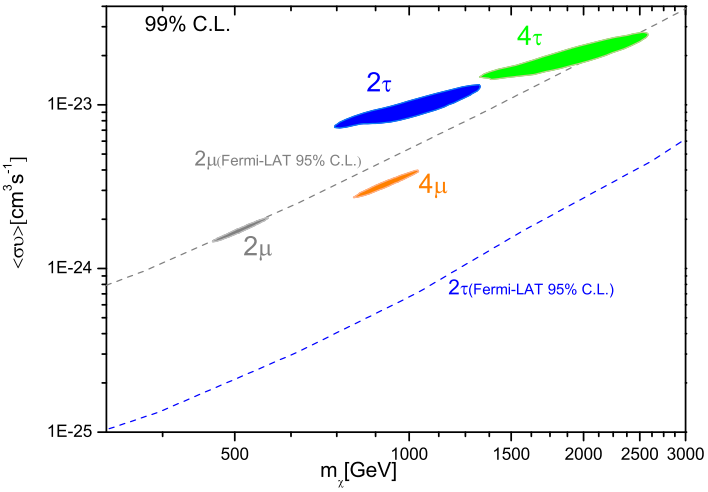

Figure 6. Allowed regions for DM particle mass and annihilation cross section at 99% CL for DM annihilation into 2μ, 4μ, 2τ and 4τ final states from the global fit. The upper limits on the 2μ and 2τ channels from the Fermi-LAT 6-year gamma-ray data of the dwarf spheroidal satellite galaxies of the Milky Way are also shown [75].

arriving at the detectors, which makes the proton/antiproton fluxes more sensitive to the propagation parameters.

In the previous section, we have shown that with the current AMS-02 data the important propagation parameters such as D_0/Z_h and Z_h can be determined with better precisions, which is useful in improving the predictions for the cosmic-ray antiproton fluxes induced from DM interactions. In this section, we estimate the uncertainties in the prediction for antiproton flux from DM annihilation and construct reference propagation models which give rise to the typically minimal, median and maximal antiproton fluxes within 95% CL. Such reference models are useful for a quick estimation of the propagation uncertainties in future analyses. We shall focus only on the case of DM annihilation. It is straight forward to extend the analysis to the case of DM decay.

For a concrete illustration, we consider a reference DM model with $m_\chi = 130\,\mathrm{GeV}$, and a typical WIMP annihilation cross section $\langle\sigma v\rangle_0 = 3\times10^{-26}\,\mathrm{cm^3 s^{-1}}$ with final state dominated by $b\bar{b}$. From the propagation models allowed by the recent AMS-02 data at 95% CL, we select reference models which give minimal, median and maximal antiproton fluxes. The values of the parameters are listed in table 3, and the corresponding fluxes for different types of DM profiles are shown in figure 8. As can be seen from the figure, the uncertainties due to the propagation parameters are within an order of magnitude. In some previous analysis, the choice of benchmark models leads to an uncertainty of $\mathcal{O}(100)$ [22]. Such a significant improvement is related to the precision AMS-02 data on the B/C ratio. Figure 8 also shows that the differences due to the DM profile are typically around a factor of two among the profiles of NFW, Isothermal and Einasto. In the Moore profile, the differences are bigger and can reach $\mathcal{O}(20)$.

7 Dark matter properties from current and future antiproton data

Taking into account the uncertainties of all the propagation parameters, one can derive conservative constraints on the properties of DM particles from the current PAMELA data and

JCAP09(2015)049

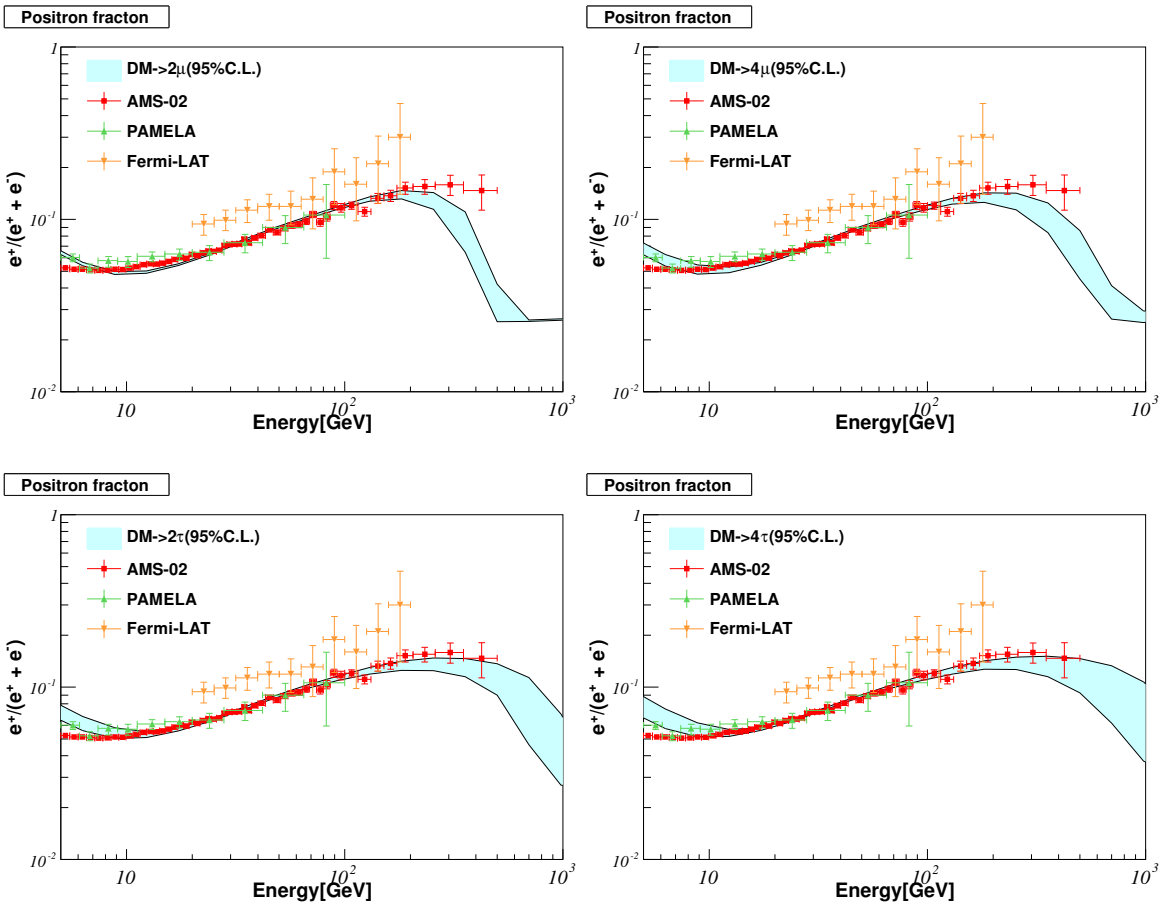

Figure 7. Predictions for cosmic-ray positron fraction from DM annihilation into final states 2μ, 4μ, 2τ and 4τ. In each plot, the shaded band represents the uncertainties due to that in the propagation parameters and the DM properties (m_χ and $\langle\sigma_v\rangle$) at 95% CL. The data of AMS-02 [2], PAMELA [4] and Fermi-LAT [5] are also shown.

parameters	Min	Med	Max
Z_h(kpc)	1.8	3.2	6.0
D_0/Z_h	1.96	2.03	1.77
δ	0.30	0.29	0.29
$V_a(\mathrm{km}\cdot\mathrm{s}^{-1})$	42.7	44.8	43.4
γ_{p1}	1.75	1.79	1.81
γ_{p2}	2.44	2.45	2.46

Table 3. Three reference propagation models selected from the set of propagation models allowed within 95% CL by the AMS-02 data, corresponding to the minimal, median and maximal antiproton fluxes from DM annihilating into $b\bar{b}$. The parameter D_0/Z_h is in units of $10^{28}\mathrm{cm}^2\cdot\mathrm{s}^{-1}\mathrm{kpc}^{-1}$.

make projections for the sensitivity of the upcoming AMS-02 antiproton measurement. Some previous analyses based on simplified assumptions of fixed background or allowing part of the propagation parameters to vary can be found in refs. [76–79]. In the Bayesian approach, it is

JCAP09(2015)049

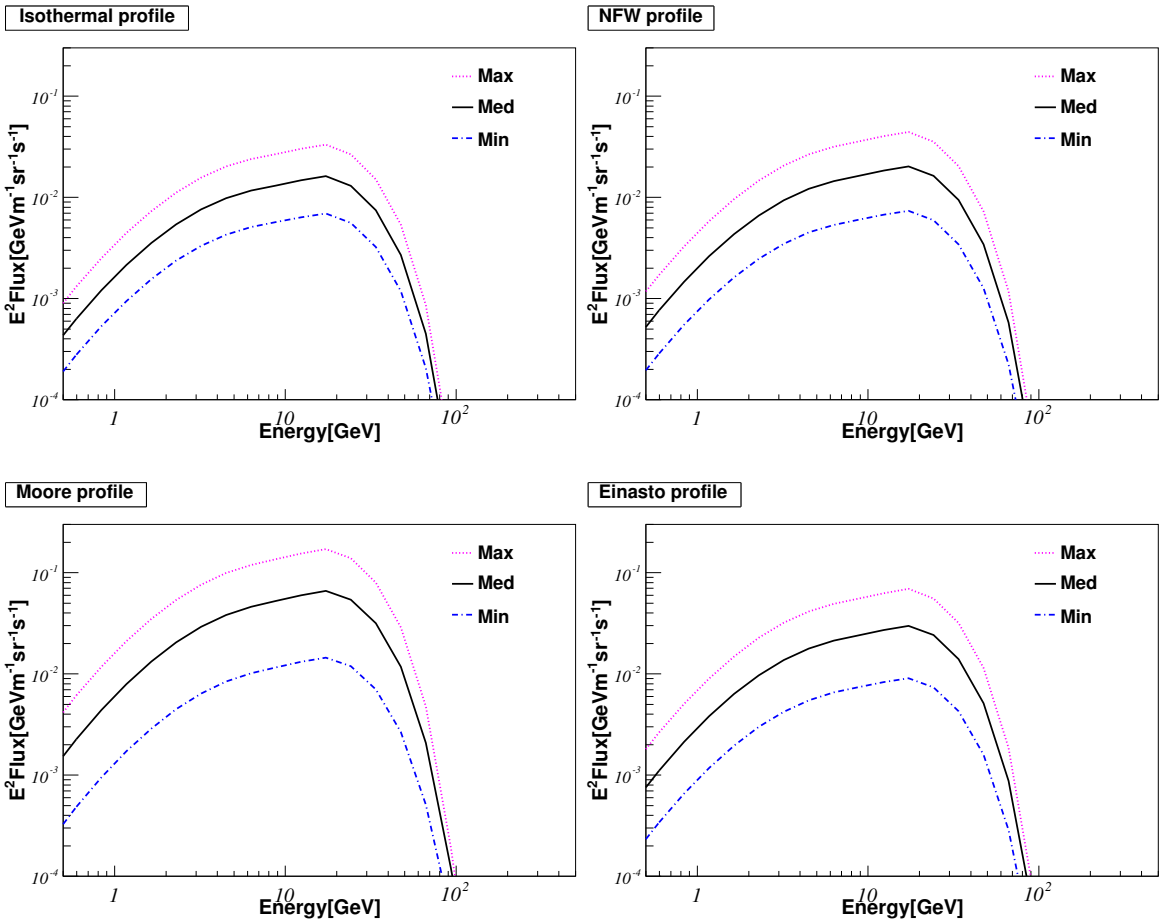

Figure 8. Prediction for the antiproton fluxes resulting from DM particle annihilating into $b\bar{b}$ final states in the three propagation models listed in table 3. In each plot, three curves correspond to the typically minimal (dot-dashed), median (solid) and maximal (dotted) antiproton fluxes at 95% CL. The four plots corresponds to the four different DM density distribution profile NFW (upper left) [40], Isothermal (upper right) [41], Moore (lower left) [42, 43] and Einasto (lower right) [44]. The mass of the DM particle is 130 GeV and the annihilation cross section is fixed at $\langle\sigma v\rangle_0 = 3\times10^{-26}\,\mathrm{cm^3 s^{-1}}$.

straightforward to consider the uncertainties and correlations of the propagation parameters consistently, as the posterior PDFs of the propagation parameters obtained in section 4 can be used as the prior PDFs in the subsequent Bayesian analysis. The inclusion of the new data will also update the "degree of believe" of these parameters, as well as constrain the new parameters related to the properties of DM particles. In the case of DM annihilation, the new parameter set related to DM annihilation is $\boldsymbol{\theta}' = \{\langle\sigma v\rangle, m_\chi\}$. The new data set of cosmic-ray antiproton is $D' = \{D_p^{\rm PAM}, D_{\bar{p}/p}^{\rm PAM}\}$, where $D_p^{\rm PAM}(D_{\bar{p}/p}^{\rm PAM})$ stands for the data of antiproton flux (antiproton to proton flux ratio) from PAMELA. The posterior PDF for the parameter set $\boldsymbol{\theta}'$ can be written as

$$P(\boldsymbol{\theta}', \boldsymbol{\theta}|D') = \frac{\mathcal{L}(D'|\boldsymbol{\theta}', \boldsymbol{\theta})\pi(\boldsymbol{\theta}')\tilde{\pi}'(\boldsymbol{\theta})}{\int \mathcal{L}(D'|\boldsymbol{\theta}', \boldsymbol{\theta})\pi(\boldsymbol{\theta}')\tilde{\pi}(\boldsymbol{\theta})d\boldsymbol{\theta}'d\boldsymbol{\theta}}, \tag{7.1}$$

where $\tilde{\pi}(\boldsymbol{\theta})$ is the prior PDF of the propagation parameter set $\boldsymbol{\theta}$ defined in eq. (4.2), which has been updated from uniform distributions after considering the constraints from the AMS-02

JCAP09(2015)049

data set D in eq. (4.1), i.e., $\tilde{\pi}(\boldsymbol{\theta}) = P(\boldsymbol{\theta}|D)$, where $P(\boldsymbol{\theta}|D)$ is calculated using the Bayes's theorem in eq. (3.1).

7.1 Constraints on DM properties from PAMELA antiproton data

We consider several reference DM annihilation channels $\bar{\chi}\chi \to X$ where $X = b\bar{b}$, $t\bar{t}$, W^+W^-, Z^0Z^0 and hh. The energy spectra of these channels are all similar at high energies. The main difference is in the average number of total antiprotons N_X per DM annihilation of each channel. For a DM particle mass $m_\chi = 500\,\mathrm{GeV}$, the values of N_X for typical final states are $N_{q\bar{q}} = 2.97$ ($q = u, d$), $N_{b\bar{b}} = 2.66$, $N_{t\bar{t}} = 3.20$, $N_{WW} = 1.42$, $N_{ZZ} = 1.48$, and $N_{hh} = 2.18$, respectively. Note that some of them are related. For instance, $N_{hh} \approx 2N_{b\bar{b}} \cdot \mathrm{Br}^2(h \to b\bar{b})$.

We include the data of antiproton flux and antiproton-to-proton flux ratio from the current PAMELA experiment [72, 74]. To avoid the complicities involved in modelling the effect of solar modulation, we only include the data points with antiproton kinetic energy $E > 10\,\mathrm{GeV}$. In total 8 (7) data points from antiproton flux (antiproton-to-proton flux ratio) are included in the analysis. The DM profile is chosen to be Einasto as a benchmark profile. Note that changes in the results with other DM profiles can be estimated from figure 8. For instance, the limits obtained for Isothermal and NFW are expected by to be slightly weaker and that for the Moore profile should more stringent.

We use the method described in eq. (7.1) to obtain the upper limits on $\langle\sigma v\rangle$ for a give value of m_χ, which takes into account of the uncertainties in the propagation parameters. Figure 9 shows the results of upper limits on the annihilation cross sections at 95% CL. The one-side 95% CL upper limit is defined as the value of the quantity below where 95% of the MCMC samples are found, which corresponds to the value 0.95 of the cumulative distribution function. When the uncertainties in the propagation parameters are included, the upper limits obtained are always above the typical thermal cross section $\langle\sigma v\rangle_0$ for the mass range $m_\chi \approx 10\,\mathrm{GeV}$–$1\,\mathrm{TeV}$. For $b\bar{b}$ final state, the most stringent limit is $\langle\sigma v\rangle \lesssim 10^{-25}\,\mathrm{cm^3 s^{-1}}$ at $m_\chi \approx 70\,\mathrm{GeV}$. For TeV scale DM particle, the upper limits are around $10^{-24}\,\mathrm{cm^3 s^{-1}}$ for all the channels. For a comparison, in figure 9 we also show the upper limits on the $b\bar{b}$ and W^+W^- channels obtained from the Fermi-LAT gamma-ray data of dwarf satellite galaxies of the Milky Way [80]. One can see from the figure that when the uncertainties in the propagation parameters are considered, the upper limits from the PAMELA $b\bar{b}$ data are slightly more stringent that from the gamma-ray data.

7.2 Projected AMS-02 sensitivity

The forthcoming AMS-02 data on the antiproton flux is eagerly awaited. The AMS-02 detector has a high rejection power to distinguish antiprotons from protons, which is extremely helpful in identifying small excesses in the antiproton fluxes. In this section, we investigate the prospect for AMS-02 on reconstructing the property of DM particle in the case where an excess in the cosmic-ray antiproton flux over the conventional astrophysical background is identified in the forthcoming AMS-02 antiproton data.

We generate mock data of antiproton flux according to the specifications of the AMS-02 detector for the case of an astrophysical background plus a contribution from DM annihilation into $b\bar{b}$ final states. The binning of the kinetic energy spectrum of the antiproton flux is based on the rigidity resolution of the AMS-02 detector which is obtained through fitting to the figure 2 of ref. [81]

$$\frac{\Delta R}{R} = 0.000477 \times R + 0.103. \tag{7.2}$$

JCAP09(2015)049

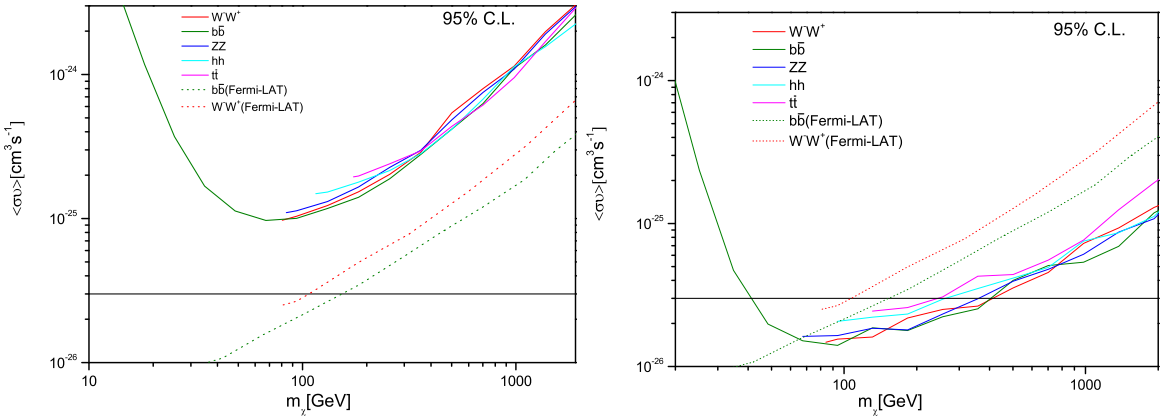

Figure 9. Left) upper limits on the cross sections for DM particle annihilating into $b\bar{b}$, W^+W^-, Z^0Z^0, hh and $t\bar{t}$ final states at 95% CL with the uncertainties in the propagation models taken into account. The DM halo profile is assumed to be Einasto. The horizontal line indicates the typical thermal DM annihilation cross section $\langle\sigma v\rangle_0 = 3 \times 10^{-26}\,\mathrm{cm^3 s^{-1}}$. The upper limits on the $b\bar{b}$ and W^+W^- channels from the Fermi-LAT 6-year gamma-ray data of dwarf spheroidal satellite galaxies of the Milky Way are also shown [75]. Right) the same as left, but for the mock data corresponding to the AMS-02 three-year data taking, assuming background only.

This value is for the observed event tracks hitting on both layer-1 and layer-9 of the AMS-02 silicon tracker. The rigidity resolution reaches 100% for $R \approx 1.9$ TV, which roughly sets the upper limit on the proton/antiproton rigidity that can be measured by the AMS-02 detector. The relation between the resolution of the kinetic energy T and that of the rigidity reads

$$\frac{\Delta T}{T} = \left(\frac{T + 2m_p}{T + m_p}\right)\frac{\Delta R}{R}, \tag{7.3}$$

where m_p is the proton mass. The expected number of antiprotons N in the i-th kinetic energy bin with kinetic energy T_i for an exposure time Δt is given by

$$N = \epsilon a(T_i)\phi(T_i)\Delta T_i \Delta t, \tag{7.4}$$

where ϵ is the efficiency of the detector, $a(T_i)$ is the acceptance for antiproton at kinetic energy T_i, $\phi(T_i)$ is the expected antiproton flux, and ΔT_i is the width of the i-th kinetic energy bin. From ref. [82], the acceptance is $a(T) \approx 0.147\,\mathrm{m^2}$ for $1\,\mathrm{GeV} \leq T \leq 11\mathrm{GeV}$ and $a(T) \approx 0.03\,\mathrm{m^2}$ for $11\,\mathrm{GeV} \leq T \leq 150\,\mathrm{GeV}$. For $T \geq 150\,\mathrm{GeV}$, the acceptance drops very quickly with increasing kinetic energy. In numerical calculations, we interpolate the values of $a(T)$ from figure 8 of ref. [82]. The efficiency is assumed to be a constant $\epsilon = 0.9$ in this work. Due to the geomagnetic effects, the value of ϵ becomes very low at kinetic energies below 1 GeV [83], we thus only consider the mock data above 1 GeV.

Under the assumption that the distribution of the observed antiproton events is Poissonian, the statistic uncertainty in N observed events is $\Delta N = \sqrt{N}$. Thus the statistic uncertainty in the flux $\phi(T_i)$ is

$$\Delta\phi(T_i)_{\mathrm{sta}} = \sqrt{\frac{\phi(T_i)}{\epsilon a(T_i)\Delta T_i \Delta t}}. \tag{7.5}$$

The systematic uncertainties may have various sources, such as the misidentification of background protons and electrons as antiprotons. The AMS-02 detector has a rejection power

JCAP09(2015)049

of $p : \bar{p} \sim 10^5$–10^6 for protons and $e^- : \bar{p} \sim 10^3$–10^4 for electrons. At multi-GeV energy region, the flux ratios of $p/\bar{p}$ and $e^-/\bar{p}$ are $\sim 10^4$ and $\sim 10^2$ respectively. Thus the systematic uncertainty can reach $\sim$ 1–10%. In this work, we take the systematic uncertainty to be $\Delta\phi_{\rm sys} = 8\%$. The total uncertainty is $\Delta\phi(T_i) = \sqrt{\Delta\phi(T_i)^2_{\rm sta} + \Delta\phi^2_{\rm sys}}$.

In figure 10, we show the mock data of the projected AMS-02 antiproton flux with 3-year data taking. The antiproton background is generated according to the best-fit propagation parameters listed in table 2. We assume that the DM particles annihilate into $b\bar{b}$ final states with a typical thermal cross section $\langle\sigma v\rangle_0 = 3 \times 10^{-26}\,{\rm cm^3 s^{-1}}$ for different masse $m_\chi = 10$, 100, 250 and 500 GeV, respectively, and the cases of large cross sections $\langle\sigma v\rangle = 1$ and $3 \times 10^{-25}\,{\rm cm^3 s^{-1}}$ for a large $m_\chi = 500\,{\rm GeV}$. The halo DM profile is assumed to be Einasto. As can be seen from the figure, only in the cases where a light 10 GeV DM particle with typical thermal cross section or a heavy 500 GeV DM particle with a large cross section, the DM contribution can lead to a visible change in the antiproton flux. However, it is still possible that a tiny change in the spectrum of antiproton flux can be identified by the AMS-02 experiment. We first consider the case without DM contribution, i.e., the future AMS-02 data is consistent with the background. In this case, upper limits can be derived as a function of m_χ as it is done for the PAMELA data. We follow the same treatment to apply a 10 GeV cut to the mockdata as in the case of PAMELA. The result as shown in the right panel of figure 9 indicates that much stronger limits can be obtained for the AMS-02 three-year data taking, which can be compatible with that from the current Fermi-LAT gamma data. We then investigate the reconstruction capability for two specific cases in the Einasto and NFW profiles. In one case the DM annihilation cross section is fixed to the standard thermal cross section, i.e., $\langle\sigma v\rangle = \langle\sigma v\rangle_0$ and the DM particle mass is allowed to vary in the range $\sim$ 10–500 GeV. In figure 11, we show the results of the reconstruction for $m_\chi = 10$, 30, 50, 100, 250 and 500 GeV, respectively. The figure shows that for $m_\chi \lesssim 100\,{\rm GeV}$, the annihilation cross section can be reconstructed with uncertainties about a factor of two for both Einasto and NFW profiles. For a fixed annihilation cross section, the reconstruction becomes difficult for heavier DM particle, as the source term is suppressed by m_χ^2. As shown in figure 11, when $m_\chi > 250\,{\rm GeV}$, only an upper limit is obtained from the mock data. In the other case, the DM particle mass m_χ is fixed at 500 GeV and $\langle\sigma v\rangle$ differs significantly from $\langle\sigma v\rangle_0$. For large annihilation cross sections $\langle\sigma v\rangle = 1 \times 10^{-25}\,{\rm cm^2}$ and $3 \times 10^{-25}\,{\rm cm^2}$, we find that the cross section can still be well reconstracted with uncertainty typically about a factor of two. In both the cases, we find that the DM particle mass can be well reconstructed with uncertainties less than $\sim 30\%$.

8 Conclusions

The AMS-02 experiment is measuring the spectra of cosmic-ray nuclei fluxes with unprecedented accuracies, which is of crucial importance in understanding the origin and propagation of the cosmic rays and searching for dark matter. We have performed a global Bayesian analysis of the constraints on the cosmic-ray propagation models from the recent AMS-02 data on the ratio of Boron to Carbon nuclei and proton flux with the assumption that the primary source is a broken power law in rigidity. The analysis is based on the method of MCMC sampling. The result has shown that the propagation parameters can be well determined by the AMS-02 data alone. For instance, the ratio of the diffusion coefficient to the diffusive halo height is found to be $D_0/Z_h \simeq 2.0\,{\rm cm^2 s^{-1} kpc^{-1}}$ with uncertainty less than 5%. The best-fit value of the halo width is $Z_h \simeq 3.3$ kpc with uncertainty less than 50%. Other parameters

JCAP09(2015)049

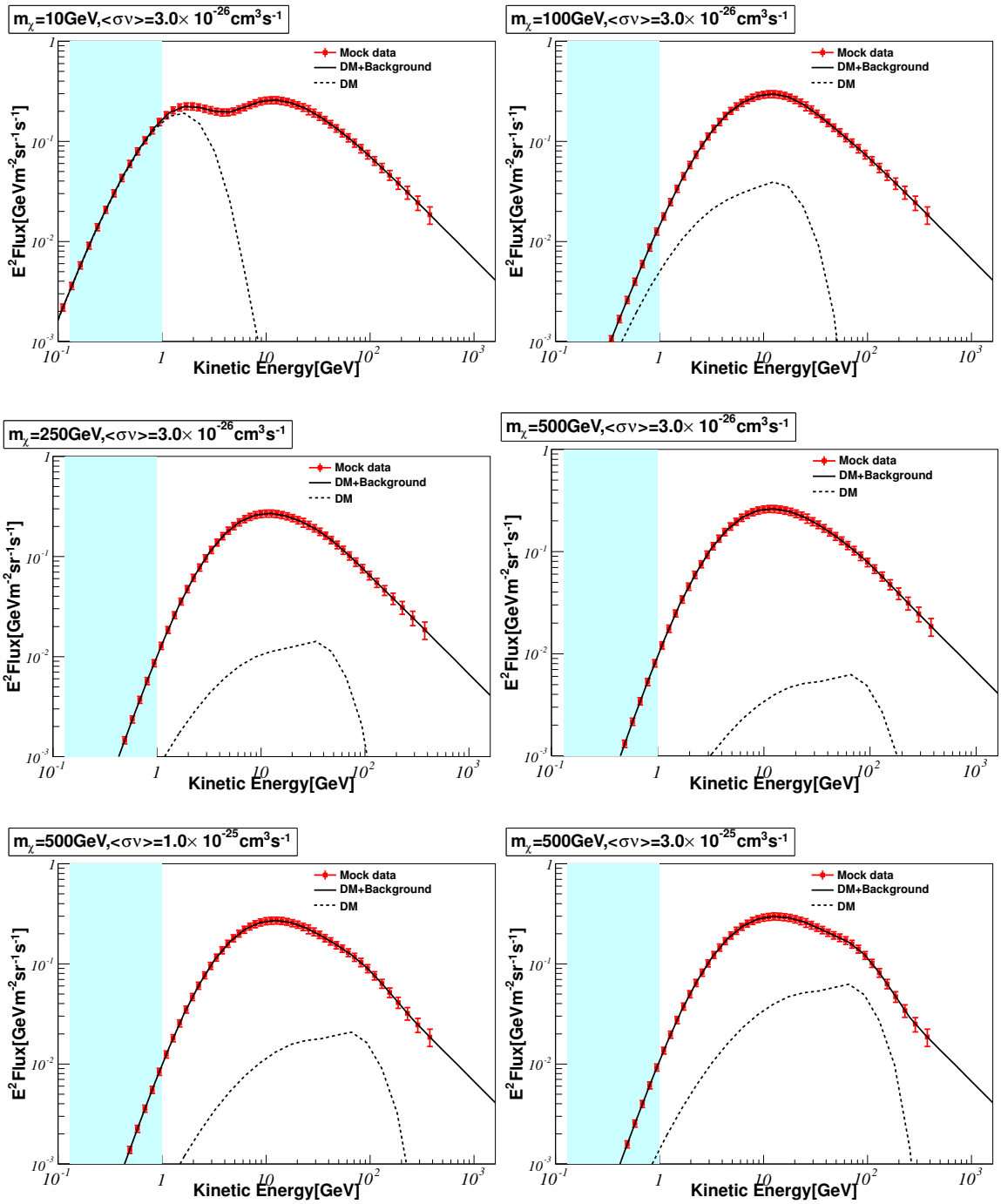

Figure 10. Mock data of the projected AMS-02 antiproton flux with 3 years of data taking in the assumption of DM annihilating into $b\bar{b}$ final states with a typical thermal cross section $\langle\sigma v\rangle_0 = 3\times10^{-26}\,\mathrm{cm^3 s^{-1}}$ for DM particle masse $m_\chi = 10$, 100, 250, 500 GeV, respectively, and the cases of large cross sections $\langle\sigma v\rangle = 1$ and $3\times10^{-25}\,\mathrm{cm^3 s^{-1}}$ for $m_\chi = 500$ GeV. In each plot, the dashed line represents the contribution from DM only, and the solid line represents the sum of background and DM contribution. The background is generated from the best-fit propagation parameters shown in table 2. The halo DM profile is assumed to be Einasto. The mock data with kinetic energy below 1 GeV (shadowed region) is not used for the reconstruction of DM properties due to the geomagnetic cut off of the detection efficiency.

JCAP09(2015)049

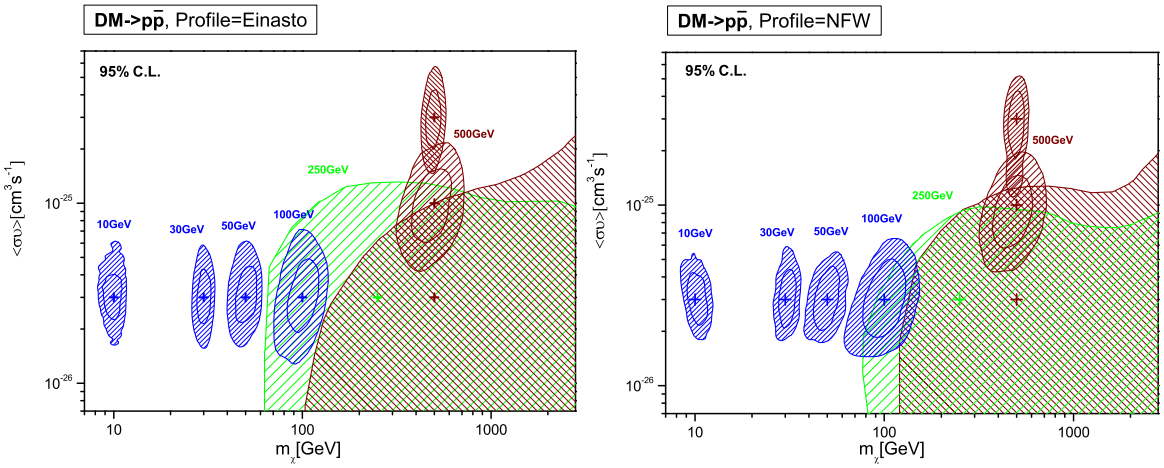

Figure 11. (Left) reconstructed allowed regions of DM particle mass and annihilation cross section at 68% and 95% CLs from the mock data of antiproton flux. The mock data correspond to the projected AMS-02 antiproton flux with 3 years of data taking in the assumption of DM annihilating into $b\bar{b}$ final states with a typical thermal cross section $\langle\sigma v\rangle_0 = 3\times10^{-26}\,\mathrm{cm^3 s^{-1}}$ for DM particle masses $m_\chi = 10$, 30, 50, 100, 250 and 500 GeV, and the cases of large cross sections $\langle\sigma v\rangle = 1$ and $3\times10^{-25}\,\mathrm{cm^3 s^{-1}}$ for $m_\chi = 500\,\mathrm{GeV}$. The DM profile is assumed to be Einasto. Right) the same as left, but for the NFW profile.

such as the Alfvèn speed and the power law indices of the primary sources have also been determined. Such results can be used to improve the prediction of the antiproton flux from DM interactions. Using the allowed regions of parameter space, we have estimate the uncertainties in the positron fraction and antiproton fluxes predicted by DM annihilation. We have shown that the uncertainty in the predicted positron fraction is within a factor of two and that in the antiproton flux is within an order of magnitude, which are much smaller than the estimations in the previous analyses prior to AMS-02. With all the uncertainties and correlations in the propagation parameters taken into account, we have derived conservative upper limits on the cross sections for DM annihilating into various standard model final states from the current PAMELA antiproton data. We have also investigated the reconstruction capability of the future AMS-02 antiproton data on the DM properties. The result have shown that if the DM particles are lighter than 100 GeV and the annihilation cross section is the typical thermal cross section, the annihilation cross section can be well reconstructed with uncertainties around a factor of two for the AMS-02 three-year data taking.

Acknowledgments

We are grateful to S. Ting for warm hospitality and insightful discussions during our visit to the AMS-02 POCC at CERN. We thank P. Zuccon, A. Kounine, A. Oliva and S. Haino for helpful discussions on the details of the AMS-02 detector. YLW and YFZ also thank R.K. Su, Z.W. Li, Y.Q. Ma, D. Jin, X. Cai and X.M. Zhang for their strong support in the 973 program and useful discussions. This work is supported in part by the National Basic Research Program of China (973 Program) under Grants No. 2010CB833000; the National Nature Science Foundation of China (NSFC) under Grants No. 10821504, No. 10905084, No. 11335012 and No. 11475237; the numerical calculations were done using the HPC Cluster of SKLTP/ITP-CAS.

JCAP09(2015)049

References

[1] Planck collaboration, P.A.R. Ade et al., *Planck 2013 results. XVI. Cosmological parameters*, *Astron. Astrophys.* **571** (2014) A16 [arXiv:1303.5076] [INSPIRE].

[2] AMS collaboration, L. Accardo et al., *High Statistics Measurement of the Positron Fraction in Primary Cosmic Rays of* 0.5–500 *GeV with the Alpha Magnetic Spectrometer on the International Space Station*, *Phys. Rev. Lett.* **113** (2014) 121101 [INSPIRE].

[3] PAMELA collaboration, O. Adriani et al., *An anomalous positron abundance in cosmic rays with energies* 1.5–100 *GeV*, *Nature* **458** (2009) 607 [arXiv:0810.4995] [INSPIRE].

[4] O. Adriani et al., *A statistical procedure for the identification of positrons in the PAMELA experiment*, *Astropart. Phys.* **34** (2010) 1 [arXiv:1001.3522] [INSPIRE].

[5] Fermi-LAT collaboration, M. Ackermann et al., *Measurement of separate cosmic-ray electron and positron spectra with the Fermi Large Area Telescope*, *Phys. Rev. Lett.* **108** (2012) 011103 [arXiv:1109.0521] [INSPIRE].

[6] J. Kopp, *Constraints on dark matter annihilation from AMS-02 results*, *Phys. Rev.* **D 88** (2013) 076013 [arXiv:1304.1184] [INSPIRE].

[7] A. De Simone, A. Riotto and W. Xue, *Interpretation of AMS-02 Results: Correlations among Dark Matter Signals*, *JCAP* **05** (2013) 003 [arXiv:1304.1336] [INSPIRE].

[8] Q. Yuan, X.-J. Bi, G.-M. Chen, Y.-Q. Guo, S.-J. Lin and X. Zhang, *Implications of the AMS-02 positron fraction in cosmic rays*, *Astropart. Phys.* **60** (2015) 1 [arXiv:1304.1482] [INSPIRE].

[9] I. Cholis and D. Hooper, *Dark Matter and Pulsar Origins of the Rising Cosmic Ray Positron Fraction in Light of New Data From AMS*, *Phys. Rev.* **D 88** (2013) 023013 [arXiv:1304.1840] [INSPIRE].

[10] L. Feng, R.-Z. Yang, H.-N. He, T.-K. Dong, Y.-Z. Fan and J. Chang, *AMS-02 positron excess: new bounds on dark matter models and hint for primary electron spectrum hardening*, *Phys. Lett.* **B 728** (2014) 250 [arXiv:1303.0530] [INSPIRE].

[11] H.-B. Jin, Y.-L. Wu and Y.-F. Zhou, *Implications of the first AMS-02 measurement for dark matter annihilation and decay*, *JCAP* **11** (2013) 026 [arXiv:1304.1997] [INSPIRE].

[12] Z.-P. Liu, Y.-L. Wu and Y.-F. Zhou, *Sommerfeld enhancements with vector, scalar and pseudoscalar force-carriers*, *Phys. Rev.* **D 88** (2013) 096008 [arXiv:1305.5438] [INSPIRE].

[13] L. Bergstrom, T. Bringmann, I. Cholis, D. Hooper and C. Weniger, *New limits on dark matter annihilation from AMS cosmic ray positron data*, *Phys. Rev. Lett.* **111** (2013) 171101 [arXiv:1306.3983] [INSPIRE].

[14] A. Ibarra, A.S. Lamperstorfer and J. Silk, *Dark matter annihilations and decays after the AMS-02 positron measurements*, *Phys. Rev.* **D 89** (2014) 063539 [arXiv:1309.2570] [INSPIRE].

[15] C.-Q. Geng, D. Huang and L.-H. Tsai, *Imprint of multicomponent dark matter on AMS-02*, *Phys. Rev.* **D 89** (2014) 055021 [arXiv:1312.0366] [INSPIRE].

[16] M. Di Mauro, F. Donato, N. Fornengo, R. Lineros and A. Vittino, *Interpretation of AMS-02 electrons and positrons data*, *JCAP* **04** (2014) 006 [arXiv:1402.0321] [INSPIRE].

[17] S.-J. Lin, Q. Yuan and X.-J. Bi, *Quantitative study of the AMS-02 electron/positron spectra: Implications for pulsars and dark matter properties*, *Phys. Rev.* **D 91** (2015) 063508 [arXiv:1409.6248] [INSPIRE].

[18] M. Ibe, S. Matsumoto, S. Shirai and T.T. Yanagida, *Mass of Decaying Wino from AMS-02 2014*, *Phys. Lett.* **B 741** (2015) 134 [arXiv:1409.6920] [INSPIRE].

[19] Q.-H. Cao, C.-R. Chen and T. Gong, *Leptophilic Dark Matter and AMS-02 Cosmic-ray Positron Flux*, arXiv:1409.7317 [INSPIRE].

JCAP09(2015)049

[20] P. Mertsch and S. Sarkar, *AMS-02 data confront acceleration of cosmic ray secondaries in nearby sources*, *Phys. Rev.* **D 90** (2014) 061301 [arXiv:1402.0855] [INSPIRE].

[21] T. Delahaye, R. Lineros, F. Donato, N. Fornengo and P. Salati, *Positrons from dark matter annihilation in the galactic halo: Theoretical uncertainties*, *Phys. Rev.* **D 77** (2008) 063527 [arXiv:0712.2312] [INSPIRE].

[22] F. Donato, N. Fornengo, D. Maurin and P. Salati, *Antiprotons in cosmic rays from neutralino annihilation*, *Phys. Rev.* **D 69** (2004) 063501 [astro-ph/0306207] [INSPIRE].

[23] A. Putze, L. Derome and D. Maurin, *A Markov Chain Monte Carlo technique to sample transport and source parameters of Galactic cosmic rays: II. Results for the diffusion model combining B/C and radioactive nuclei*, *Astron. Astrophys.* **516** (2010) A66 [arXiv:1001.0551] [INSPIRE].

[24] R. Trotta, G. Johannesson, I.V. Moskalenko, T.A. Porter, R.R. de Austri and A.W. Strong, *Constraints on cosmic-ray propagation models from a global Bayesian analysis*, *Astrophys. J.* **729** (2011) 106 [arXiv:1011.0037] [INSPIRE].

[25] J. Liu, Q. Yuan, X.-J. Bi, H. Li and X. Zhang, *CosRayMC: a global fitting method in studying the properties of the new sources of cosmic $e^{\pm}$ excesses*, *Phys. Rev.* **D 85** (2012) 043507 [arXiv:1106.3882] [INSPIRE].

[26] K. Auchettl and C. Balázs, *Extracting the size of the cosmic electron-positron anomaly*, *Astrophys. J.* **749** (2012) 184 [arXiv:1106.4138] [INSPIRE].

[27] AMS collaboration, A. Oliva, *Precision Measurement of the Cosmic Ray Boron-to-Carbon Ratio with AMS*, in talk given at *The 33rd International Cosmic Ray Conference (ICRC2013)*, Rio de Janeiro, Brazil, 2–9 July 2013 and online at http://www.cbpf.br/∼icrc2013/papers/icrc2013-1266.pdf.

[28] AMS collaboration, S. Haino, *Precision measurement of the proton flux with AMS*, in talk given at *The 33rd International Cosmic Ray Conference (ICRC2013)*, Rio de Janeiro, Brazil, 2–9 July 2013 and online at http://www.cbpf.br/∼icrc2013/papers/icrc2013-1265.pdf.

[29] PAMELA collaboration, O. Adriani et al., *PAMELA Measurements of Cosmic-ray Proton and Helium Spectra*, *Science* **332** (2011) 69 [arXiv:1103.4055] [INSPIRE].

[30] V.S. Berezinskii, S.V. Bulanov, V.A. Dogiel and V.S. Ptuskin, *Astrophysics of cosmic rays*, North-Holland, Amsterdam The Netherlands (1990).

[31] D. Maurin, R. Taillet, F. Donato, P. Salati, A. Barrau and G. Boudoul, *Galactic cosmic ray nuclei as a tool for astroparticle physics*, astro-ph/0212111 [INSPIRE].

[32] V.S. Berezinskii, S.V. Bulanov, V.A. Dogiel and V.S. Ptuskin, *Astrophysics of cosmic rays*, North-Holland, Amsterdam (1990).

[33] A.W. Strong, I.V. Moskalenko and O. Reimer, *Diffuse continuum gamma-rays from the galaxy*, *Astrophys. J.* **537** (2000) 763 [*Erratum ibid.* **541** (2000) 1109] [astro-ph/9811296] [INSPIRE].

[34] G. Case and D. Bhattacharya, *Revisiting the galactic supernova remnant distribution*, *Astron. Astrophys. Suppl.* **120** (1996) 437.

[35] A.W. Strong and I.V. Moskalenko, *Propagation of cosmic-ray nucleons in the galaxy*, *Astrophys. J.* **509** (1998) 212 [astro-ph/9807150] [INSPIRE].

[36] FERMI-LAT collaboration, L. Tibaldo and I.A. Grenier, *Fermi observations of Cassiopeia and Cepheus: gamma-ray diffuse emission in the outer Galaxy*, arXiv:0907.0312 [INSPIRE].

[37] T. Sjöstrand, S. Mrenna and P.Z. Skands, *A Brief Introduction to PYTHIA 8.1*, *Comput. Phys. Commun.* **178** (2008) 852 [arXiv:0710.3820] [INSPIRE].

[38] P. Ilten, *Tau Decays in PYTHIA 8*, *Nucl. Phys. Proc. Suppl.* **253–255** (2014) 77 [arXiv:1211.6730] [INSPIRE].

JCAP09(2015)049

[39] P. Salucci, F. Nesti, G. Gentile and C.F. Martins, *The dark matter density at the Sun's location*, *Astron. Astrophys.* **523** (2010) A83 [arXiv:1003.3101] [INSPIRE].

[40] J.F. Navarro, C.S. Frenk and S.D.M. White, *A Universal density profile from hierarchical clustering*, *Astrophys. J.* **490** (1997) 493 [astro-ph/9611107] [INSPIRE].

[41] L. Bergstrom, P. Ullio and J.H. Buckley, *Observability of gamma-rays from dark matter neutralino annihilations in the Milky Way halo*, *Astropart. Phys.* **9** (1998) 137 [astro-ph/9712318] [INSPIRE].

[42] B. Moore et al., *Dark matter substructure within galactic halos*, *Astrophys. J.* **524** (1999) L19 [astro-ph/9907411] [INSPIRE].

[43] J. Diemand, B. Moore and J. Stadel, *Convergence and scatter of cluster density profiles*, *Mon. Not. Roy. Astron. Soc.* **353** (2004) 624 [astro-ph/0402267] [INSPIRE].

[44] J. Einasto, *Dark Matter*, arXiv:0901.0632 [INSPIRE].

[45] L.J. Gleeson and W.I. Axford, *Solar Modulation of Galactic Cosmic Rays*, *Astrophys. J.* **154** (1968) 1011 [INSPIRE].

[46] I.V. Moskalenko, A.W. Strong, J.F. Ormes and M.S. Potgieter, *Secondary anti-protons and propagation of cosmic rays in the galaxy and heliosphere*, *Astrophys. J.* **565** (2002) 280 [astro-ph/0106567] [INSPIRE].

[47] V.S. Ptuskin, I.V. Moskalenko, F.C. Jones, A.W. Strong and V.N. Zirakashvili, *Dissipation of magnetohydrodynamic waves on energetic particles: impact on interstellar turbulence and cosmic ray transport*, *Astrophys. J.* **642** (2006) 902 [astro-ph/0510335] [INSPIRE].

[48] A. Neronov, D.V. Semikoz and A.M. Taylor, *Low-energy break in the spectrum of Galactic cosmic rays*, *Phys. Rev. Lett.* **108** (2012) 051105 [arXiv:1112.5541] [INSPIRE].

[49] A.W. Strong and I.V. Moskalenko, *Models for galactic cosmic ray propagation*, *Adv. Space Res.* **27** (2001) 717 [astro-ph/0101068] [INSPIRE].

[50] I.V. Moskalenko, A.W. Strong, S.G. Mashnik and J.F. Ormes, *Challenging cosmic ray propagation with antiprotons. Evidence for a fresh nuclei component?*, *Astrophys. J.* **586** (2003) 1050 [astro-ph/0210480] [INSPIRE].

[51] F. Donato, D. Maurin, P. Salati, A. Barrau, G. Boudoul and R. Taillet, *Anti-protons from spallations of cosmic rays on interstellar matter*, *Astrophys. J.* **563** (2001) 172 [astro-ph/0103150] [INSPIRE].

[52] M. Cirelli et al., *PPPC 4 DM ID: A Poor Particle Physicist Cookbook for Dark Matter Indirect Detection*, *JCAP* **03** (2011) 051 [*Erratum ibid.* **10** (2012) E01] [arXiv:1012.4515] [INSPIRE].

[53] A. Lewis and S. Bridle, *Cosmological parameters from CMB and other data: A Monte Carlo approach*, *Phys. Rev.* **D 66** (2002) 103511 [astro-ph/0205436] [INSPIRE].

[54] F. Feroz and M.P. Hobson, *Multimodal nested sampling: an efficient and robust alternative to MCMC methods for astronomical data analysis*, *Mon. Not. Roy. Astron. Soc.* **384** (2008) 449 [arXiv:0704.3704] [INSPIRE].

[55] F. Feroz, M.P. Hobson and M. Bridges, *MultiNest: an efficient and robust Bayesian inference tool for cosmology and particle physics*, *Mon. Not. Roy. Astron. Soc.* **398** (2009) 1601 [arXiv:0809.3437] [INSPIRE].

[56] AMS collaboration, M. Aguilar et al., *Electron and Positron Fluxes in Primary Cosmic Rays Measured with the Alpha Magnetic Spectrometer on the International Space Station*, *Phys. Rev. Lett.* **113** (2014) 121102 [INSPIRE].

[57] G.O. Roberts and A.F.M. Smith, *Simple conditions for the convergence of the Gibbs sampler and Metropolis-Hastings algorithms*, *Stoch. Proc. Appl.* **49** (1994) 207.

JCAP09(2015)049

[58] J.J. Engelmann, P. Ferrando, A. Soutoul, P. Goret and E. Juliusson, *Charge composition and energy spectra of cosmic-ray for elements from Be to NI — Results from HEAO-3-C2*, *Astron. Astrophys.* **233** (1990) 96 [INSPIRE].

[59] A.D. Panov et al., *Relative abundances of cosmic ray nuclei B-C-N-O in the energy region from* 10 *GeV/n to* 300 *GeV/n. Results from ATIC-2 (the science flight of ATIC)*, arXiv:0707.4415 [INSPIRE].

[60] H.S. Ahn et al., *Measurements of cosmic-ray secondary nuclei at high energies with the first flight of the CREAM balloon-borne experiment*, *Astropart. Phys.* **30** (2008) 133 [arXiv:0808.1718] [INSPIRE].

[61] N.E. Yanasak et al., *Measurement of the secondary radionuclides* ^{10}Be, ^{26}Al, ^{36}Cl, ^{54}Mn, *and* ^{14}C *and implications for the galactic cosmic-ray age*, *Astrophys. J.* **563** (2001) 768.

[62] J.S. George et al., *Elemental composition and energy spectra of galactic cosmic rays during solar cycle 23*, *Astrophys. J.* **698** (2009) 1666.

[63] G. Di Bernardo, C. Evoli, D. Gaggero, D. Grasso and L. Maccione, *Cosmic Ray Electrons, Positrons and the Synchrotron emission of the Galaxy: consistent analysis and implications*, *JCAP* **03** (2013) 036 [arXiv:1210.4546] [INSPIRE].

[64] E. Orlando and A.W. Strong, *Galactic synchrotron emission with cosmic ray propagation models*, arXiv:1309.2947 [INSPIRE].

[65] T. Bringmann, F. Donato and R.A. Lineros, *Radio data and synchrotron emission in consistent cosmic ray models*, *JCAP* **01** (2012) 049 [arXiv:1106.4821] [INSPIRE].

[66] N. Fornengo, R.A. Lineros, M. Regis and M. Taoso, *The isotropic radio background revisited*, *JCAP* **04** (2014) 008 [arXiv:1402.2218] [INSPIRE].

[67] J. Lavalle, D. Maurin and A. Putze, *Direct constraints on diffusion models from cosmic-ray positron data: Excluding the minimal model for dark matter searches*, *Phys. Rev.* **D 90** (2014) 081301 [arXiv:1407.2540] [INSPIRE].

[68] D. Maurin, F. Donato, R. Taillet and P. Salati, *Cosmic rays below* $z = 30$ *in a diffusion model: new constraints on propagation parameters*, *Astrophys. J.* **555** (2001) 585 [astro-ph/0101231] [INSPIRE].

[69] T. Hams et al., *Measurement of the Abundance of Radioactive* ^{10}Be *and Other Light Isotopes in Cosmic Radiation up to* 2 *GeV Nucleon*$^{-1}$ *with the Balloon-borne Instrument ISOMAX*, *Astrophys. J.* **611** (2004) 892 [INSPIRE].

[70] Y.S. Yoon et al., *Cosmic-Ray Proton and Helium Spectra from the First CREAM Flight*, *Astrophys. J.* **728** (2011) 122 [arXiv:1102.2575] [INSPIRE].

[71] A. Davis et al., *On the low energy decrease in galactic cosmic ray secondary/primary ratios*, *AIP Conf. Proc.* **528** (2000) 421.

[72] PAMELA collaboration, O. Adriani et al., *PAMELA results on the cosmic-ray antiproton flux from* 60 *MeV to* 180 *GeV in kinetic energy*, *Phys. Rev. Lett.* **105** (2010) 121101 [arXiv:1007.0821] [INSPIRE].

[73] K. Abe et al., *Measurement of the cosmic-ray antiproton spectrum at solar minimum with a long-duration balloon flight over Antarctica*, *Phys. Rev. Lett.* **108** (2012) 051102 [arXiv:1107.6000] [INSPIRE].

[74] O. Adriani et al., *A new measurement of the antiproton-to-proton flux ratio up to* 100 *GeV in the cosmic radiation*, *Phys. Rev. Lett.* **102** (2009) 051101 [arXiv:0810.4994] [INSPIRE].

[75] FERMI-LAT collaboration, M. Ackermann et al., *Searching for Dark Matter Annihilation from Milky Way Dwarf Spheroidal Galaxies with Six Years of Fermi-LAT Data*, arXiv:1503.02641 [INSPIRE].

JCAP09(2015)049

[76] I. Cholis, *New Constraints from PAMELA anti-proton data on Annihilating and Decaying Dark Matter*, *JCAP* **09** (2011) 007 [arXiv:1007.1160] [INSPIRE].

[77] C. Evoli, I. Cholis, D. Grasso, L. Maccione and P. Ullio, *Antiprotons from dark matter annihilation in the Galaxy: astrophysical uncertainties*, *Phys. Rev.* **D 85** (2012) 123511 [arXiv:1108.0664] [INSPIRE].

[78] M. Cirelli and G. Giesen, *Antiprotons from Dark Matter: Current constraints and future sensitivities*, *JCAP* **04** (2013) 015 [arXiv:1301.7079] [INSPIRE].

[79] N. Fornengo, L. Maccione and A. Vittino, *Constraints on particle dark matter from cosmic-ray antiprotons*, *JCAP* **04** (2014) 003 [arXiv:1312.3579] [INSPIRE].

[80] FERMI-LAT collaboration, M. Ackermann et al., *Dark matter constraints from observations of 25 Milky Way satellite galaxies with the Fermi Large Area Telescope*, *Phys. Rev.* **D 89** (2014) 042001 [arXiv:1310.0828] [INSPIRE].

[81] AMS collaboration, P. Zuccon, *AMS-02 Track reconstruction and rigidity measurement*, in talk given at *The 33rd International Cosmic Ray Conference (ICRC2013)*, Rio de Janeiro, Brazil, 2–9 July 2013 and online at http://www.cbpf.br/∼icrc2013/papers/icrc2013-1064.pdf.

[82] AMS collaboration, A.G. Malinin, *Astroparticle physics with AMS-02*, *Phys. Atom. Nucl.* **67** (2004) 2044 [INSPIRE].

[83] R. Battiston, *XVI Lomonosov Conference on Elementary Particle Physics*, Moscow State University, Moscow, Russia, 22–28 August 2013.

JCAP09(2015)049